

CP violating signal at DUNE in presence of nonstandard interactions and the role of second oscillation maxima

Rajrupa Banerjee[†] [1](#), Jogesh Rout[‡] [2](#), Sudhanwa Patra[†] [3](#), Poonam Mehta* [4](#)

[†] *Department of Physics, Indian Institute of Technology Bhilai, Durg 491002, India*

[‡] *Department of Physics, Shree Ram College, Rampur, Subarnapur, Odisha 767045, India*

[‡] *Institute of Physics, Bhubaneswar, Sachivalaya Marg, Bhubaneswar 751005, India*

**School of Physical Sciences, Jawaharlal Nehru University, New Delhi 110067, India*

Abstract

Neutrino oscillation among the three active neutrino flavors is well established and supported by experiments at diverse length scales and energy scales. It may be noted that five of the neutrino oscillation parameters in the three-flavor paradigm, namely the three mixing angles (θ_{12} , θ_{13} , θ_{23}) and the two mass-squared differences (Δm_{21}^2 , Δm_{31}^2) are measured to a reasonable degree of precision. The three unknowns that are expected to be deciphered in the near future are the Dirac CP phase, δ , the neutrino mass ordering, and the octant of θ_{23} . The next generation of long baseline experiments, such as the Deep Underground Neutrino Experiment (DUNE), aims to resolve these unanswered questions. In the present work, by considering DUNE as an example, we assess the ability of long baseline experiments to extricate the intrinsic contribution from observables related to CP violation in scenarios considering SI and beyond. Additionally, we analyze the role of the second oscillation maximum in addressing the above mentioned questions. By carrying out event level and statistical analyses, we assess the potential of DUNE to probe CP violation effects both within and beyond the standard paradigm.

¹rajrupab@iitbhilai.ac.in

²jogesh.rout1@gmail.com

³sudhanwa@iitbhilai.ac.in

⁴pm@jnu.ac.in

1 Introduction

The idea of neutrino oscillations was proposed by Pontecorvo, Maki, Nakagawa, and Sakata [1–5]. Neutrino oscillations imply that neutrinos possess tiny masses and undergo flavor transitions during propagation. Since neutrinos are assumed to be massless within the Standard Model (SM), the discovery of neutrino oscillations provides us with an unprecedented opportunity to probe physics beyond the SM [6]. Much of the data from various neutrino oscillation experiments can be explained by invoking the standard paradigm of three neutrino mixing (see [7–9] for recent global analyses of oscillation data). There are also some anomalous results that cannot be reconciled within the standard three neutrino paradigm. This calls for other possibilities beyond the minimal framework needed to explain neutrino mass and mixing. Among various possible explanations, the idea of non-standard interactions (NSI) of neutrinos (see [10] for a review) and additional sterile neutrino states (see [11] for a review) have been widely explored in the literature. Other scenarios, such as violation of Lorentz invariance and CPT symmetry, have also been invoked [12].

In the standard three neutrino paradigm, the neutrino oscillation framework has nine flavor parameters (three masses, three mixing angles, and three phases) - five of these (three angles and two mass-squared differences) have been measured to a fair degree of precision, as is evident from the global analyses of data [7–9]. Neutrino oscillations are insensitive to the two Majorana phases and the absolute scale of the neutrino mass. The three angles ($\theta_{12}, \theta_{13}, \theta_{23}$) and the Dirac CP phase (δ) appear in the 3×3 leptonic mixing matrix, commonly referred to as the Pontecorvo-Maki-Nakagawa-Sakata (PMNS) matrix [13]. In vacuum, δ induces CP and T violation effects, and we shall refer to these as intrinsic or real CP effects. Since matter is CP asymmetric, additional CP violating effects may be induced during propagation in matter, making it difficult to infer the true value of the CP phase that appears in the mixing matrix. These effects are termed extrinsic or fake as they hinder the determination of the intrinsic CP phase. Determining whether CP violation occurs in the leptonic sector is of fundamental importance. This phenomenon could provide a crucial insight into the mechanisms behind the observed matter-antimatter asymmetry in the universe, potentially through the process of leptogenesis [14, 15].

Some of the upcoming long baseline neutrino experiments, such as the DUNE [16–18], T2HK [19], T2HKK [20], P2O [21, 22] etc are promising as these will allow us to measure the three unknowns - the value of the Dirac CP phase (δ), the sign of (Δm_{32}^2) or the mass ordering and the octant of θ_{23} . The primary objective of DUNE is to probe CP violation in the neutrino sector [16–18]. In its experimental configuration, a high purity wide band muon neutrino beam is produced at Fermilab, which traverses a baseline of 1300 km to reach a liquid argon (LAr) far detector situated on axis at the Sanford Underground Research Facility. DUNE uniquely allows us to study the first oscillation maximum as well as the second oscillation maximum of $\nu_\mu \rightarrow \nu_e$ oscillation probability [23–25]. This aids in enhanced sensitivity to CP violation effects.

NSI of neutrinos was first introduced in the seminal paper by Wolfenstein [26]. Several phenomenological studies have been carried out exploring the impact of NSI on the

determination of CP violation, mass ordering, and octant of θ_{23} at various experiments, including the long baseline neutrino experiments [27–61]. In the present work, we shall restrict ourselves to the NSI only, though there is a body of work dealing with other new physics scenarios such as sterile neutrinos [11]. In theoretical frameworks, nine independent non-standard interaction (NSI) parameters, each accompanied by an associated complex phase, are expected to exist in nature. Current experimental data from various neutrino oscillation experiments [12, 62, 63] provide constraints on the allowed magnitudes and phases of these NSI parameters [64–67].

It is known that there are inherent difficulties in elucidating whether CP is violated in the neutrino sector, even in the case where there are no new interactions. In the presence of NSI [40, 43] or sterile neutrinos [68, 69], the problem of disentangling is more pronounced (see, for instance, [53, 68] for separation of physics scenarios employing different beam tunes at DUNE). Possible ways have been suggested which allow us to separate the intrinsic and extrinsic sources of CP violation both in the presence of NSI and light sterile neutrinos [52, 68]. In the above backdrop, it is evident that one needs to re-look at these questions, keeping in mind the experimental flexibility achievable, for instance, being able to access the second oscillation maxima in addition to the first. In the present work, we (a) study the impact of NSI on CP violation by examining the role played by the first and second oscillation maxima, (b) address the question of disentangling the intrinsic effects from extrinsic effects in the standard paradigm as well as NSI, and (c) assess the ability of considered long baseline experiments to distinguish between the two scenarios (standard versus NSI).

The structure of this paper is as follows. In Section 2, we outline the theoretical framework. This includes a detailed review of the electron neutrino appearance probability $P_{\mu e}$ in vacuum, matter with SI, and matter with NSI. We also discuss the oscillation maxima of $P_{\mu e}$, CP asymmetry, and provide a way to distinguish between intrinsic and extrinsic contributions to the CP violation. In the next Section 3, we describe the experimental and simulation details along with the description of detector specifications and experimental inputs relevant to the analysis. Section 4 is dedicated to a discussion of event rates in the DUNE experiment, focusing on their implications for CP violation studies. In Section 5, we present our primary results, including sensitivity to CP violation, the resolution of δ , and the fractional CP sensitivity, analyzed in terms of $\Delta\chi^2$. We conclude in Section 6.

2 Theoretical Framework

NSI of neutrinos can lead to neutrino oscillations even for massless neutrinos [26]. Most of the phenomenological studies on neutrino oscillations pertain to the case of vector NSI [40, 43, 44, 52, 53, 70] (see [10, 12] for reviews) while in recent times, the case of scalar NSI has also been investigated [54, 58–61]. In the present work, we shall consider vector NSI. Typically, NSI can be due to charged current (CC) or neutral current (NC) processes. Due to the stringent constraints on parameters governing CC NSI [67], we shall only consider

NC NSI. The NC NSI Lagrangian is given by [35]

$$\mathcal{L}_{NSI}^{NC} = 2\sqrt{2}G_F \sum_{\alpha, \beta, P} \epsilon_{\alpha\beta}^{f,P} \left(\bar{\nu}_\alpha \gamma^\mu P \nu_\beta \right) \left(\bar{f} \gamma_\mu P f \right). \quad (2.1)$$

Where $P \in \{P_R, P_L\}$, $P_{R,L} = (1 \mp \gamma^5)/2$, P_R and P_L are the right and left handed chirality operators, respectively, α and β corresponds to different neutrino flavors, $l_\beta = e, \mu, \tau$ while $f \in \{e, u, d\}$ denotes the possible fermion fields. The strength of NC NSI, measured by the dimensionless coefficient $\epsilon_{\alpha\beta}^f$ is defined relative to the weak interaction coupling G_F i.e. $\epsilon_{\alpha\beta}^{f,P} \sim \mathcal{O}(G_x/G_F)$. The effective Hamiltonian in the presence of NSI is

$$\hat{H} = \left[\frac{1}{2E} U \begin{pmatrix} 0 & 0 & 0 \\ 0 & \Delta m_{21}^2 & 0 \\ 0 & 0 & \Delta m_{31}^2 \end{pmatrix} U^\dagger + V_{CC} \begin{pmatrix} 1 + \varepsilon_{ee} & \varepsilon_{e\mu} & \varepsilon_{e\tau} \\ \varepsilon_{e\mu}^* & \varepsilon_{\mu\mu} & \varepsilon_{\mu\tau} \\ \varepsilon_{e\tau}^* & \varepsilon_{\mu\tau}^* & \varepsilon_{\tau\tau} \end{pmatrix} \right]. \quad (2.2)$$

The commonly adopted form of the mixing matrix U (referred to as the PMNS mixing matrix) is [13]

$$U = \begin{pmatrix} c_{12}c_{13} & s_{12}c_{13} & s_{13}e^{-i\delta_{CP}} \\ -s_{12}c_{23} - c_{12}s_{13}s_{23}e^{i\delta_{CP}} & c_{12}c_{23} - s_{12}s_{13}s_{23}e^{i\delta_{CP}} & c_{13}s_{23} \\ s_{13}s_{23} - c_{12}s_{13}c_{23}e^{i\delta_{CP}} & -c_{12}s_{23} - s_{12}s_{13}c_{23}e^{i\delta_{CP}} & c_{23}c_{13} \end{pmatrix},$$

where, $c_{ij} = \cos \theta_{ij}$ and $s_{ij} = \sin \theta_{ij}$ (with $i, j = 1, 2, 3$). While NSI parameters are generally complex, we restrict our analysis to real values within a range of positive and negative values. Additionally, using charge neutrality ($N_p = N_e$) and the quark structure of protons and neutrons, the fermion densities can be expressed as $N_u(x) = 2N_p(x) + N_n(x)$ and $N_d(x) = N_p(x) + 2N_n(x)$ these yield an expression for the NSI parameters $\varepsilon_{\alpha\beta}(x)$

$$\epsilon_{\alpha\beta}(x) = \epsilon_{\alpha\beta}^e + (2 + Y_n(x)) \epsilon_{\alpha\beta}^u + (1 + 2Y_n(x)) \epsilon_{\alpha\beta}^d, \quad (2.3)$$

where, $Y_n = N_n(x)/N_e(x)$. Although the Standard Model framework provides a well-established description of neutrino interactions, the possible presence of NSI offers a valuable probe into physics beyond the SM, such as new heavy or light mediator scenarios. NSI can significantly modify the Mikheyev-Smirnov-Wolfenstein (MSW) matter effects, thereby influencing the flavor evolution of neutrinos as they propagate through matter. This modification introduces potential challenges in precisely determining the standard oscillation parameters. In particular, the extraction of the leptonic CP violating phase, δ , becomes notably more difficult. In long baseline experiments, δ , within the standard three-flavor framework, can become entangled with additional CP-violating phases originating from NSI, which leads to ambiguities in data interpretation and standard parameter estimation.

2.1 Brief review of $\Delta P_{\mu e}^{CP}$ in NSI

To investigate the manifestation of CP violation in the presence of NSI, particularly in the context of the long baseline experiment DUNE, we focus on the electron appearance probability channel, $P_{\nu_\mu \rightarrow \nu_e}$. Using perturbative expansions available in the literature [31, 35, 55], the probability can be approximated as the sum of three leading-order contributions,

$$P_{\mu e} \simeq P_0 + P_1 + P_2. \quad (2.4)$$

Standard oscillation parameters			
Parameter	Best-fit value NO (IO)	3σ range NO (IO)	Relative uncertainty
θ_{12}	$33.68^\circ (33.68^\circ)$	$31.63^\circ \rightarrow 35.95^\circ$	2.1%
θ_{13}	$8.52^\circ (8.58^\circ)$	$8.18^\circ \rightarrow 8.87^\circ (8.24^\circ \rightarrow 8.91^\circ)$	1.3%(1.3%)
θ_{23}	$48.5^\circ (48.6^\circ)$	$41.0^\circ \rightarrow 50.5^\circ$	3.4%
$\Delta m_{21}^2 (\text{eV}^2)$	$7.49 \times 10^{-5} (7.49 \times 10^{-5})$	$6.92 \rightarrow 8.05$	2.5%
$\Delta m_{31}^2 (\text{eV}^2)$	$2.534 \times 10^{-3} (-2.484 \times 10^{-3})$	$2.451 \rightarrow 2.578 (-2.547 \rightarrow -2.421)$	0.8%(0.8%)
GLOB-OSC with NSI in ES+ ν NS			
NSI Parameter	Central value	2σ range	3σ range
$\varepsilon_{e\mu}$	0.05	$-0.12 \rightarrow +0.011$	$-0.18 \rightarrow +0.08$
$\varepsilon_{e\tau}$	-0.05	$-0.16 \rightarrow +0.083$	$-0.25 \rightarrow +0.33$
ε_{ee}	-	$-0.19 \rightarrow +0.20$	$-0.23 \rightarrow +0.25$

Table 1: Best-fit and 3σ ranges of standard oscillation parameters and NSI parameters (put ε_{ee} in table too) [36, 57, 67, 71]

Where the terms P_0 and P_1 correspond to the standard three-flavor oscillation terms in the presence of matter, while P_2 encapsulates the corrections induced by NSI effects. In this expression, the matter potential is characterized by the dimensionless parameter $|v| = |V_{CC}/k_{31}| \sim 0.22$ ($E/2.5$ GeV), with $k_{31} \cong \Delta m_{31}^2/2E$. The NSI contribution enters through the complex parameter $|\varepsilon|$, which is taken to be of the order of $\mathcal{O}(\varepsilon)$. Expanding the probability, retaining terms up to third order, we obtain the following expression for the leading order contribution to the probability in the presence of NSI [35, 72].

$$\begin{aligned} P_0 &\simeq 4s_{13}^2 s_{23}^2 f^2, \\ P_1 &\simeq 8s_{13}s_{12}c_{12}s_{23}c_{23}\alpha f g \cos(\Delta + \delta), \\ P_2 &\simeq 8s_{13}s_{23}v|\varepsilon|[af^2 \cos(\delta + \phi) + bfg \cos(\Delta + \delta + \phi)], \end{aligned} \quad (2.5)$$

where $\Delta \equiv \Delta m_{31}^2/4E$ is the atmospheric oscillation frequency related to the baseline L . The dominant term in the appearance probability $P_{\mu e}$ depends on the atmospheric mass-squared splitting Δm_{31}^2 . As a result, the key experimental features of a long-baseline $\nu_\mu \rightarrow \nu_e$ appearance measurement are determined by the baseline L and the neutrino energy E , through the ratio $1.27 \Delta m_{31}^2 L/E$. The condition for the oscillation maxima of $P_{\mu e}$ is obtained from the leading term, which yields

$$\frac{L}{E} \sim (2n - 1) \times 500 \frac{\text{km}}{\text{GeV}}, \quad (2.6)$$

Where $n = 1, 2, \dots$ correspond to the first, second, and higher oscillation maxima occurring at $L/E \sim 500, 1500, \dots$ km/GeV, respectively. For the DUNE baseline of $L = 1300$ km, this relation places the first and second oscillation maxima at approximately $E_I \simeq 2.6$ GeV, $E_{II} \simeq 0.86$ GeV. Given the smallness of the mixing angle θ_{13} and the parameter $\alpha = \Delta m_{21}^2/\Delta m_{31}^2 = 0.03$ [55] in the case of normal hierarchy, we limit our analysis to a first order approximation in the $\alpha - s_{13}$ expansion. This approach enables us to capture the

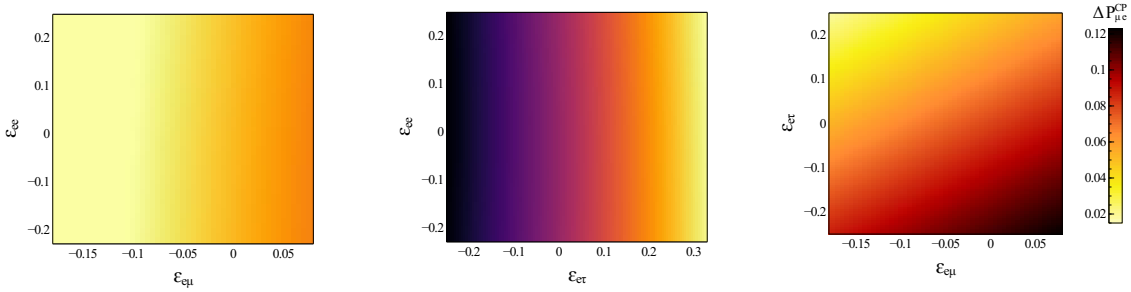


Figure 1: The oscillogram plot of variation of CP violation parameter $\Delta P_{\mu e}^{CP}$ with different NSI parameter. The left most panel depicts the dependency of $\Delta P_{\mu e}^{CP}$ with ε_{ee} and $\varepsilon_{e\mu}$, middle panel represents the variation od the CP violation with ε_{ee} and $\varepsilon_{e\tau}$ and the right panel depicts the same with the variation of $\varepsilon_{e\mu}$ and $\varepsilon_{e\tau}$.

leading contributions while maintaining computational tractability, as higher order terms contribute negligibly due to the small values of α and θ_{13} . Following [35], we introduce the functions:

$$f \equiv \frac{\sin[(1-v)\Delta]}{1-v} \quad \text{and} \quad g \equiv \frac{\sin v\Delta}{v}. \quad (2.7)$$

The term P_0 is positive definite, independent of CP phases, and provides the major contribution from the matter effect to the probability. The second term, P_1 , corresponds to the standard three-flavor interference between the solar and atmospheric oscillation frequencies, and is sensitive to the intrinsic CP violating phase, δ . The third term, P_2 , encapsulates the contribution from non-standard interactions (NSI). This term involves the complex NSI coupling and contributes only in the presence of matter, i.e., when $v \neq 0$. The NSI parameter is generally expressed as

$$\varepsilon = |\varepsilon| e^{i\phi}. \quad (2.8)$$

Where $|\varepsilon|$ denotes the magnitude of the NSI parameters and ϕ is the associated phase. The explicit form of the coefficients a and b depends on the specific flavor structure of the NSI coupling. For the two most relevant off-diagonal NSI parameters, the expressions are given by

$$a = s_{23}^2, \quad b = c_{23}^2 \quad \text{if} \quad \varepsilon = |\varepsilon_{e\mu}| e^{i\phi_{e\mu}}, \quad (2.9)$$

$$a = s_{23}c_{23}, \quad b = -s_{23}c_{23} \quad \text{if} \quad \varepsilon = |\varepsilon_{e\tau}| e^{i\phi_{e\tau}}. \quad (2.10)$$

Thus, the structure of P_2 differs slightly between the $\varepsilon_{e\mu}$ and $\varepsilon_{e\tau}$ cases, reflecting the distinct interference patterns these couplings introduce in the oscillation probability. In Eq. (2.5), the signs of Δ , α , and v are positive for the normal ordering and negative for the inverted ordering. However, a detailed investigation under the inverted mass ordering remains an open avenue for future study. In the present work, we restrict our analysis to

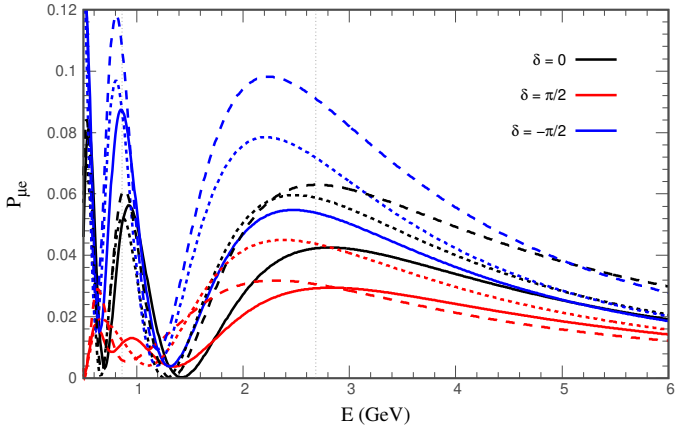


Figure 2: ν_e appearance probability in vacuum (solid lines), in presence of standard matter effect (dotted lines) and with non-standard interactions (dashed lines) with $\delta = 0, \pi/2, -\pi/2$.

the normal mass ordering scenario. Also, Eq. (2.5) is valid for neutrinos. For antineutrinos, the parameters δ and v are associated with a negative sign.

It is important to emphasize that all numerical results presented in this work are obtained using the standard neutrino oscillation parameters from the NuFIT v6.0 global fit, as listed in Table 1. The non-standard interaction (NSI) parameters are taken within their allowed 3σ ranges, also summarized in Table 1. The reason behind the specific choice of central values for the NSI parameters is illustrated in Fig. 1, where the oscillogram plots are made at the first oscillation maximum.

1. The leftmost panel displays the variation of $\Delta P_{\mu e}^{CP}$ as a function of ε_{ee} and $\varepsilon_{e\mu}$. It is evident that $\Delta P_{\mu e}^{CP}$ is largely sensitive to $\varepsilon_{e\mu}$, with a negligible contribution arising from ε_{ee} . The enhancement of CP violation is particularly pronounced for positive values of $\varepsilon_{e\mu}$.
2. The middle panel shows the dependence of $\Delta P_{\mu e}^{CP}$ on ε_{ee} and $\varepsilon_{e\tau}$. Consistent with the previous observation, the plot confirms that $\Delta P_{\mu e}^{CP}$ remains nearly unaffected by variations in ε_{ee} , while displaying a significant dependence on $\varepsilon_{e\tau}$, especially for negative values of it.
3. The rightmost panel presents the joint dependence of $\Delta P_{\mu e}^{CP}$ on both $\varepsilon_{e\mu}$ and $\varepsilon_{e\tau}$. From this plot, it becomes clear that the benchmark choice $\varepsilon_{e\mu} = 0.05$ and $\varepsilon_{e\tau} = -0.05$ provides a representative scenario for probing significant CP violating effects within the three-flavor neutrino oscillation framework. For the CP violation sensitivity analysis, however, these parameters are systematically varied within their respective 3σ bounds, in accordance with the most recent global constraints on NSI couplings as given in Table 1 [67].

Fixing the NSI parameters to $\varepsilon_{e\mu} = 0.05$ and $\varepsilon_{e\tau} = -0.05$, we analyze the energy dependence of the electron appearance probability $P_{\mu e}$ under three distinct scenarios: vacuum oscillations, standard interactions (SI), and non-standard interactions (NSI). The results are shown in Fig. 2 for three representative values of the CP phase, $\delta = 0^\circ, +90^\circ$, and -90° . The black curve corresponds to $\delta = 0^\circ$, while the red and blue curves illustrate the cases for $\delta = +90^\circ$ (cyan curve) and $\delta = -90^\circ$ (orange curve), respectively. A clear hierarchical behavior is observed in all cases: the probability $P_{\mu e}$ increases successively from vacuum (solid line) to SI (dotted line) and further to NSI (dashed line). This enhancement is more pronounced at the second oscillation maximum than at the first. In particular, for $\delta = -90^\circ$, $P_{\mu e}$ increases from approximately 0.09 in vacuum to about 0.125 in the presence of NSI. This pronounced rise indicates that the second oscillation maximum offers enhanced sensitivity to CP-violating effects. Moreover, the substantial modification of $P_{\mu e}$ induced by NSI underscores their potential to amplify CP sensitivity beyond that achieved within the standard three-flavor framework. A detailed discussion of this enhanced CP sensitivity and its phenomenological implications is presented in the subsequent sections.

2.2 $\Delta P_{\mu e}^{CP}$ in NSI

The appearance probability, including NSI, can be expressed in terms of three components:

$$P_0 \simeq \underbrace{4s_{13}^2 s_{23}^2 f^2}_I, \quad (2.11)$$

$$P_1 \simeq \underbrace{8s_{13}s_{12}c_{12}s_{23}c_{23}\alpha f g \cos(\Delta + \delta)}_{II}, \quad (2.12)$$

$$P_2 \simeq \underbrace{8s_{13}s_{23}v|\varepsilon|[af^2 \cos(\delta + \phi) + bf g \cos(\Delta + \delta + \phi)]}_{III}, \quad (2.13)$$

Terms I and II represent purely fake CP contributions and admixture of extrinsic and intrinsic CP effects due to SI with the matter potential, respectively, while term III introduces additional contributions from NSI parameters. In simplified and compact form, the CP violation expression in the presence of NSI is expressed as,

$$\begin{aligned} \Delta P_{\mu e}^{CP} = \Phi & \left[\frac{\Phi}{4} (f^2 - f'^2) + v(f^2 + f'^2)(\varepsilon_{e\mu} - \xi) \cos \delta \right. \\ & \left. + g(x + y)(f' + f) \cos \Delta \cos \delta + g(x - y)(f' - f) \sin \Delta \sin \delta \right] \end{aligned}$$

where $\Phi = 4s_{13}s_{23}$, $x = v(\varepsilon_{e\mu} + \xi)$, $y = \alpha \sin 2\theta_{12} \cos \theta_{23}$, $\xi = \varepsilon_{e\mu} \cos 2\theta_{23} - \varepsilon_{e\tau} \sin 2\theta_{23}$, $f = \sin(1 - v)\Delta/(1 - v) = 0.22E/2.5$, $f' = \sin(1 + v)\Delta/(1 + v) = -0.22E/2.5$, $g = \sin v\Delta/v$. The expression for the CP violation term in the presence of NSI reveals that, unlike the SI effect, NSI introduces a $\cos \delta$ dependency that is independent of the oscillation maxima. This implies that, at the oscillation maxima, in addition to the sinusoidal dependence on δ observed in vacuum and SI scenarios, an additional $\cos \delta$ dependent term emerges uniquely due to NSI that restrict $\Delta P_{\mu e}^{CP}$ to approach absolute zero at the CP conserving regions i.e. $\delta = 0, \pm\pi$. Since neutrino oscillation experiments primarily focus

on the region near the oscillation maximum, one can set $\sin \Delta = 1$. Consequently, at the oscillation maximum, the expression for $\Delta P_{\mu e}^{CP}$ simplifies to the following form,

$$\Delta P_{\mu e}^{CP} = \Phi \left[\frac{\Phi}{4} \left(f^2 - f'^2 \right) + v \left(f^2 + f'^2 \right) (\varepsilon_{e\mu} - \xi) \cos \delta + g (x - y) (f' - f) \sin \delta \right]. \quad (2.14)$$

However, since the $\cos \delta$ term is coupled with both the matter potential and NSI parameters, a reduction in the contribution from the matter effect allows the impact of NSI to be observed more prominently. The higher order oscillation maxima enable this possibility of minimizing the matter effect to explore the enhanced NSI contribution in three flavor neutrino oscillation.

2.3 Extraction of CP violating phase in presence of NSI

After examining the CP violating effects analytically in vacuum, in matter, and in the presence of NSI, we now investigate the possibility of extracting the intrinsic CP violation from the admixture of intrinsic and extrinsic contributions. By separating these components and rearranging the terms in the CP asymmetry expression, we obtain $\Delta P_{\mu e}^{CP} = P_{\mu e} - \bar{P}_{\mu e}$ as shown in Eq. (2.15).

$$\begin{aligned} \Delta P_{\mu e}^{CP} = & \underbrace{4s_{13}^2 s_{23}^2 (f^2 - (f')^2)}_{\text{Extrinsic}} \\ & + \underbrace{8s_{13}s_{23}s_{12}c_{12}c_{23}\alpha g [\cos \delta \cos \Delta (f + f') + \sin \Delta \sin \delta (f - f')]}_{\text{Extrinsic and Intrinsic CP violation due to matter effect}} \\ & + \underbrace{8s_{13}s_{23}v|\varepsilon| [a \cos \delta (f^2 + f'^2) + bg \{\cos \Delta \cos \delta (f + f') + \sin \Delta \sin \delta (f' - f)\}]}_{\text{Extrinsic and Intrinsic CP violation due to matter effect and NSI}}. \end{aligned} \quad (2.15)$$

The contributions can be grouped according to their dependence on the CP phase:

1. *Term containing $\sin \Delta \sin \delta$:* These encode a combination of intrinsic and extrinsic CP violation, with contributions originating from both matter effects and NSI. Since the factor $\sin \Delta$ peaks at the oscillation maxima, this term remains nonzero at these points and therefore captures the dominant CP violating behavior near the second oscillation maximum.
2. *Term containing $\cos \Delta \cos \delta$:* These terms also represent mixed intrinsic-extrinsic CP violation arising from matter and NSI. However, because $\cos \Delta$ vanishes at the oscillation maxima, their contribution is suppressed at these points. As a result, they play no role in the regions of maximal oscillation probability.
3. *Term containing $\cos \delta$:* These contributions are also an entangled effect of both intrinsic and extrinsic CP violation due to matter and NSI effects. Since they do not depend on the oscillation phase Δ , they remain nonzero regardless of the oscillation maxima and are independent of the location of the oscillation peaks.

Hence, it is evident that the term proportional to $\cos \delta$ arises exclusively in the presence of NSI, as it originates from the NSI induced modification of the matter potential. In the absence of NSI, the only surviving genuine CP violating contribution is the term proportional to $\sin \Delta \sin \delta$, which represents the standard intrinsic CP violation. The potential for observing CP violating effects becomes particularly significant near the second oscillation maximum, as clearly illustrated in the oscillogram of $\Delta P_{\mu e}^{CP}$ over the whole (E, δ) parameter space. All numerical results and figures presented in this work are generated using the General Long Baseline Experiment Simulator (GLoBES) software [73, 74]. The simulations incorporate complete three-flavor neutrino propagation in matter, using the PREM density profile [75] along with the oscillation parameter values listed in Table 1. Fig. 3 shows the oscillograms for the vacuum, matter, and NSI scenarios. The orange and blue regions indicate large CP asymmetry, reaching values of order 0.1, highlighting the enhanced sensitivity achievable at the second oscillation maximum, especially when NSI effects are included. To elucidate these features in detail, we now examine the oscillogram structure in the three scenarios shown in Fig. 3.

1. **Vacuum:** The leftmost panel of Fig. 3 displays the CP asymmetry in vacuum. As expected from Fig. 2, maximal CP violation occurs at $\delta = \pm 90^\circ$, while CP violation vanishes at $\delta = 0^\circ$ and 180° . The oscillogram also shows that large CP asymmetry can occur at higher order oscillation maxima. Although higher maxima provide stronger sensitivity, only the first and second oscillation maxima lie within the accessible energy range of DUNE. In vacuum, the CP asymmetry can reach magnitudes of approximately 0.1, representing purely intrinsic CP violation, unaffected by matter effects.
2. **SI:** The middle panel demonstrates how matter effects modify the vacuum pattern. The symmetry observed in vacuum is significantly distorted, particularly around the first oscillation maximum. A region of strong CP asymmetry (visible as a dark orange patch) appears near the first oscillation minimum, a feature entirely absent in vacuum, indicating the role of matter induced (extrinsic) CP violation. The region of large CP asymmetry at the second oscillation maximum also expands in the presence of matter, although a partial symmetry is still retained there. This partial preservation makes the second oscillation maximum particularly valuable for disentangling the intrinsic CP effect from the extrinsic CP effect, maximizing the possibility of extracting δ .
3. **NSI:** The rightmost panel shows the oscillogram when NSI are included. NSI causes an even stronger distortion of the symmetry seen in vacuum, especially around the first oscillation maximum, where the symmetry is almost completely broken. The magnitude of CP violation is noticeably enhanced compared to the SI case, reflecting the additional interference introduced by NSI parameters. In contrast, the second oscillation maximum retains partial symmetry and continues to exhibit a pronounced region of large CP asymmetry. This behavior indicates that the second oscillation maximum not only provides improved sensitivity to large CP violation in the presence

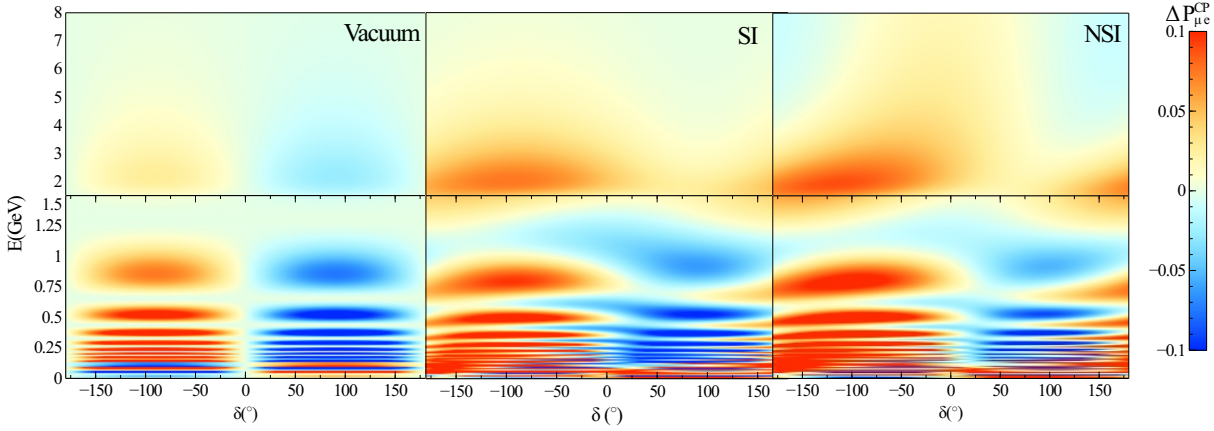


Figure 3: The oscillogram plot presented in the figure illustrates the dependence of the CP violation factor $\Delta P_{\mu e}^{CP}$ on the δ . The left panel of the figure represents the scenario in vacuum, where $\Delta P_{\mu e}^{CP}$ exhibits a purely intrinsic CP violation effect, manifesting a symmetric behavior between the maximal and minimal CP violation regions. This symmetry indicates that $\Delta P_{\mu e}^{CP}$ is exclusively governed by the intrinsic CP phase, without external influences. In the presence of standard matter interactions, as shown in the middle panel, the symmetry of $\Delta P_{\mu e}^{CP}$ is significantly distorted. As a result, the extraction of intrinsic CP violation becomes increasingly challenging when transitioning from the vacuum scenario to the matter affected regime. The right panel of the figure further explores the impact of NSI on $\Delta P_{\mu e}^{CP}$. The inclusion of NSI exacerbates the difficulty in isolating the intrinsic CP violation component. Despite this complication, NSI significantly enhances the maximum CP violation values, suggesting that while the extraction of intrinsic CP violation is hindered, the overall magnitude of CP violation is amplified.

of NSI but also offers a more favorable environment for untwining δ from extrinsic fake CP effect.

Consequently, the second oscillation maximum emerges as one of the most promising regions for evaluating δ in long-baseline setups, such as DUNE. A clearer understanding of these features emerges when examining the two dimensional dependence of $\Delta P_{\mu e}^{CP}$ on the CP phase δ at the two accessible oscillation maxima. Fig. 4 illustrates how the CP asymmetry varies with δ at first and second oscillation maxima, enabling a direct comparison between vacuum, standard matter effects, and NSI contributions. The main observations from the figure are summarized below.

- **Oscillation Maxima:** The red curves correspond to the first oscillation maximum, while the blue curves represent the second. Dotted lines depict vacuum oscillations, dashed lines include standard matter effects, and solid lines incorporate NSI. The light-shaded bands indicate the shift from intrinsic CP behavior due to matter effects, whereas the darker shades highlight the additional deviation introduced by NSI.
- **Relative Magnitudes:** Across all scenarios, the magnitude of $\Delta P_{\mu e}^{CP}$ is consistently larger at the second oscillation maximum (E^{II}) than at the first (E^I), for both SI and NSI cases.
- **Amplitude Enhancement:** The value of $\Delta P_{\mu e}^{CP}$ at the second maximum is amplified by nearly a factor of three relative to the first in the presence of NSI. This highlights the increased sensitivity of the second maximum to CP violating effects.

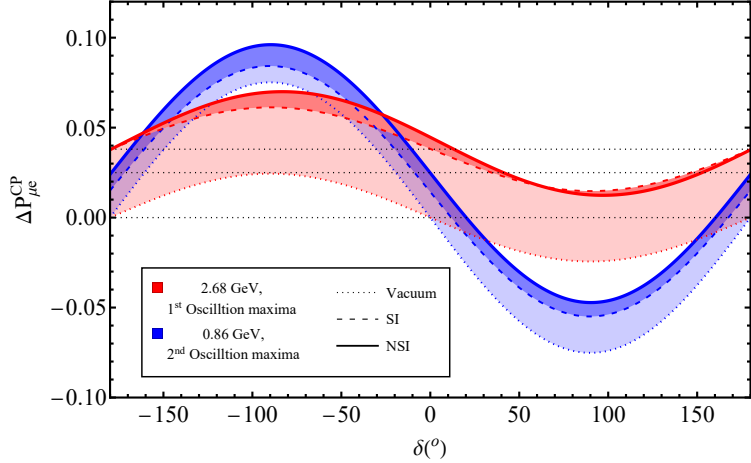


Figure 4: The figure illustrates the variation of the CP violation factor $\Delta P_{\mu e}^{CP}$ as a function of δ for different oscillation scenarios: vacuum (dotted line), standard matter effects (dashed line), and the presence of NSI (solid line). The red curves correspond to the first oscillation maximum at 2.68 GeV, while the blue curves represent the second oscillation maximum at 0.86 GeV. The shaded region highlights the excess contribution to CP violation arising from matter effects and NSI, beyond the intrinsic CP violation component. The plot demonstrates the amplification of CP violation effects due to matter interactions and NSI, with a stronger influence observed at the second oscillation maximum.

- **Peak Behavior:** The largest differences occur near $\delta = \pm 90^\circ$. The maximum value of $\Delta P_{\mu e}^{CP}$ reaches approximately 0.1037 at $\delta = -90^\circ$, observed for both SI and NSI at an energy of 0.86 GeV.
- **CP Conserving Phases:** For CP conserving values ($\delta = 0^\circ$ or $\pm 180^\circ$), $\Delta P_{\mu e}^{CP}$ vanishes in vacuum at both E^I and E^{II} . In contrast, matter effects and NSI produce a nonzero asymmetry in these regions. In the NSI case, $\Delta P_{\mu e}^{CP}$ reaches 0.049 at $\delta = 0^\circ$ and 0.043 at $\delta = 180^\circ$.
- **Offset Due to Matter:** At the first oscillation maximum, the offset between vacuum and matter induced asymmetry is substantial. This offset becomes noticeably smaller at the second oscillation maximum, making the latter less susceptible to fake CP effects.
- **Symmetry Features:** NSI distorts the symmetry of the CP asymmetry curve around the first oscillation maximum. However, near the second maximum, the NSI induced modification is almost symmetric, effectively adding a nearly constant shift to the matter induced behavior.

Collectively, these features demonstrate that the second oscillation maximum, especially when NSI are present, provides a more favorable environment for probing and disentangling CP violating effects in neutrino oscillations. The analytical discussion above shows that the second oscillation maximum provides a substantially stronger signal of CP violation

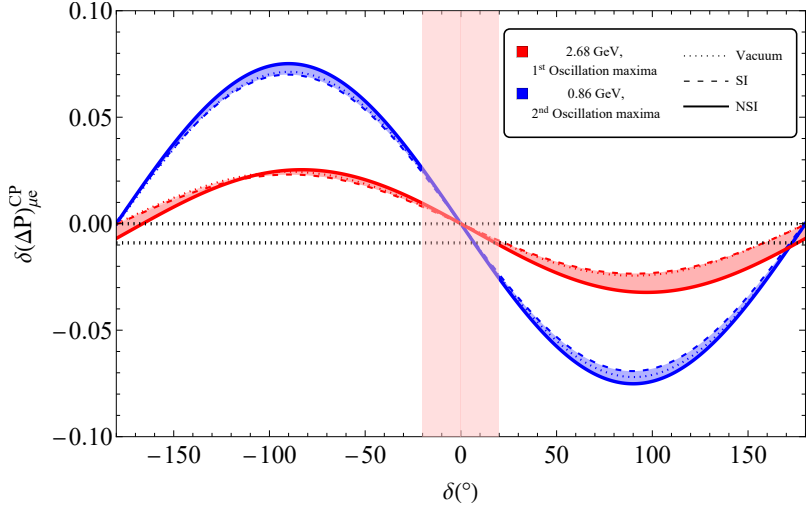


Figure 5: The same plot as Fig. 4, now presented with the parameter $\delta(\Delta P_{\mu e}^{CP}) = \Delta P_{\mu e}^{CP}(\delta) - \Delta P_{\mu e}^{CP}(\delta = 0)$. This specific parameterization is employed to analyze the contribution of fake CP violation by considering the minimal value of the intrinsic CP phase. The approach allows for a more precise assessment of the impact of matter effects and NSI on CP violation, aiding in the disentanglement of intrinsic and extrinsic contributions [57].

compared to the first. This enhancement becomes particularly striking in the presence of NSI.

2.4 Importance of higher order oscillation maxima in distinguishing intrinsic CP effects

Building on the analytical discussion above, it is evident that the second oscillation maximum plays a particularly important role in enhancing the sensitivity to CP violation, especially in the presence of NSI. In this section, we therefore focus on the prospects for extracting the CP phase δ at the second oscillation maximum.

A useful quantity for distinguishing intrinsic CP violation from extrinsic contributions (arising from matter effects or NSI) is the difference

$$\delta(\Delta P_{\mu e}^{CP}) = \Delta P_{\mu e}^{CP}(\delta) - \Delta P_{\mu e}^{CP}(\delta = 0), \quad (2.16)$$

which isolates the dependence on the CP violating phase by subtracting the CP conserving reference value. To get over the problem of finding the source of CP violation (i.e. whether due to intrinsic CP phase and due to the matter effects), the observables $\delta(\Delta P_{\mu e}^{CP})$ have been introduced which can prove useful to establish whether CP violation effects arise purely due to intrinsic CP phase or a combination of intrinsic and extrinsic CP effects. This particular choice of observable $\delta(\Delta P_{\mu e}^{CP})$ enables us to examine the possibility of extracting the information about the intrinsic CP phase. Subtracting the factor $\Delta P_{\mu e}^{CP}(\delta = 0)$ may eliminate the fake CP effect arising due to the purely matter effect. The remaining effects in the expression of CP violation are due to the intrinsic δ . However, in the presence of NSI, due to the presence of the matter dependence term $(f^2 + f'^2)$, associated with $\cos \delta$, interference from fetching the absolute intrinsic δ . This matter effect can be minimized if

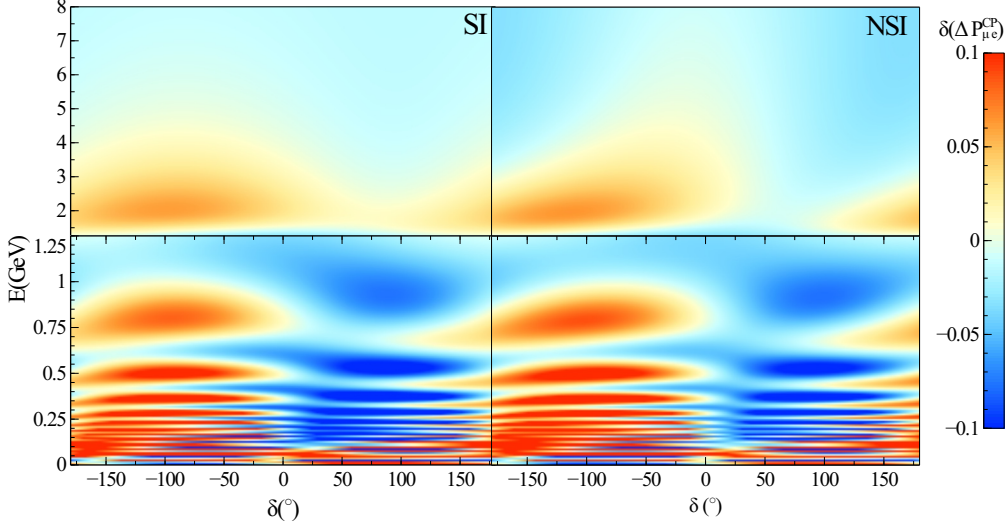


Figure 6: Oscillogram plot for $\delta(\Delta P_{\mu e}^{CP}) = \Delta P_{\mu e}^{CP}(\delta) - \Delta P_{\mu e}^{CP}(\delta = 0)$ in $E(\text{GeV})$ - $\delta(^{\circ})$ plane for standard matter effect (left panel) and NSI (right panel)

we probe the observable at the region where the matter effect is minimal, which can be achieved at the second oscillation maximum.

Fig. 5 shows the behaviour of the observable $\delta(\Delta P_{\mu e}^{CP})$ as a function of the CP phase δ for energies corresponding to the first and second oscillation maxima, for DUNE. The red curves correspond to the second oscillation maximum, while the blue curves represent the first. For each case, the dotted, dashed, and solid lines indicate the vacuum, standard matter, and NSI scenarios, respectively. The pink shaded region identifies the parameter space, for $\delta = \pm 20^{\circ}$, where the extraction of the intrinsic CP phase remains feasible even in the presence of NSI. The red and blue shaded bands highlight the deviation from pure intrinsic CP violation induced by matter effects at the second and first oscillation maxima, respectively. The plot clearly shows that this deviation is minimized where the vacuum and NSI curves nearly overlap, indicating that the second oscillation maximum provides a more favorable regime for isolating the intrinsic CP phase.

At the first oscillation maximum, around 2.68 GeV, the quantity $\Delta P_{\mu e}^{CP}$ exhibits a strong $\cos \delta$ type behaviour induced by matter effects, making it difficult to isolate the intrinsic CP phase. This matter induced contribution is substantially reduced at higher order maxima, where $\Delta P_{\mu e}^{CP}$ regains an approximately sinusoidal dependence on δ . Consequently, the interference from the $\cos \delta$ terms is suppressed at the second oscillation maximum, allowing for a clearer and more robust determination of the CP phase.

This trend is clearly illustrated in Fig. 5. At the first oscillation maximum (blue curve), the SI case (dashed line) coincides with the vacuum prediction (dotted line) at the CP-conserving point $\delta = 0^{\circ}$, but the NSI curve (solid line) deviates significantly from both at $\delta = \pm 180^{\circ}$. This behavior indicates that, while the first maximum may still be suitable for extracting δ in the SI scenario, the residual matter induced contribution from NSI prevents a clean separation of intrinsic and extrinsic effects in this region.

In contrast, at the second oscillation maximum (red curve), all three scenarios. Vacuum, SI, and NSI, converge at the CP conserving values $\delta = 0^\circ$ and $\pm 180^\circ$. This near perfect overlap demonstrates that the matter induced contamination is almost completely suppressed, even in the presence of NSI. As a result, the second oscillation maximum emerges as the most favorable region for extracting the intrinsic CP phase without significant interference from matter or NSI effects.

The oscillogram plots in Fig. 6 reinforce this conclusion even more clearly. Both the SI and NSI cases retain, to some extent, the characteristic features of the vacuum oscillogram. In particular, the approximate symmetry around the point of maximal CP violation at $\delta = 90^\circ$ is still visible, especially in the region of the second oscillation maximum. Taken together, these observations highlight that, even in the presence of NSI, the second oscillation maximum offers a more reliable and experimentally accessible region for extracting the intrinsic CP phase. This makes it a particularly advantageous setting for precision studies of leptonic CP violation.

3 Experiment and Simulation details

DUNE [16, 76] is designed as a next generation long baseline accelerator neutrino experiment, with neutrinos traveling approximately 1300 km from Fermilab to the far detector located deep underground at the Sanford Underground Research Facility in South Dakota. Beyond the standard three-flavor oscillation scenario, DUNE’s long baseline also makes it highly sensitive to possible NSI. As per the discussion in Section 2, NSI can generate parameter degeneracies such as mixing the standard CP phase δ with NSI phases and thereby shift or reduce DUNE’s apparent sensitivity to CP violation [43]. Also, the second oscillation maximum may play a crucial role in getting the CP violation sensitivity and disentangling the intrinsic contribution from the extrinsic for both SI and NSI scenarios. Therefore, we use the GLoBES framework [73, 74] together with the NSI analysis tool [77] for performing the simulations. We assume a 40 kton liquid argon time projection chamber (LArTPC) as the far detector. The TDR beam design employs 120 GeV protons at 1.2 MW beam power, corresponding to an annual exposure of 1.1×10^{21} protons on target (POT), which explores the first oscillation maximum, whereas the 8 GeV beam explores the second oscillation maximum with 3 MW power, yielding 40.1×10^{21} POT per year. The 120 GeV beam seems to be optimized around 2.5 GeV, i.e., near the first oscillation maximum, and the 8 GeV beam seems to be optimized around the second oscillation maximum. The muon-neutrino flux in neutrino (solid line) and antineutrino (dotted line) modes is shown in Fig. 7, where the red and blue curves denote the 120 GeV and 8 GeV beams, respectively. We adopt a balanced runtime of 3.5 years each in neutrino and antineutrino modes, leading to exposures of about 336 and 840 kton-MW-years for the 120 GeV and 8 GeV beams, respectively. Notably, the staged seven-year TDR run also achieves a total exposure of 336 Kton-MW-years [17]. The details of systematic uncertainties and detection efficiencies for the TDR configurations are available in Refs. [76].

For all our numerical simulations, we employ a constant Earth matter density of $\rho =$

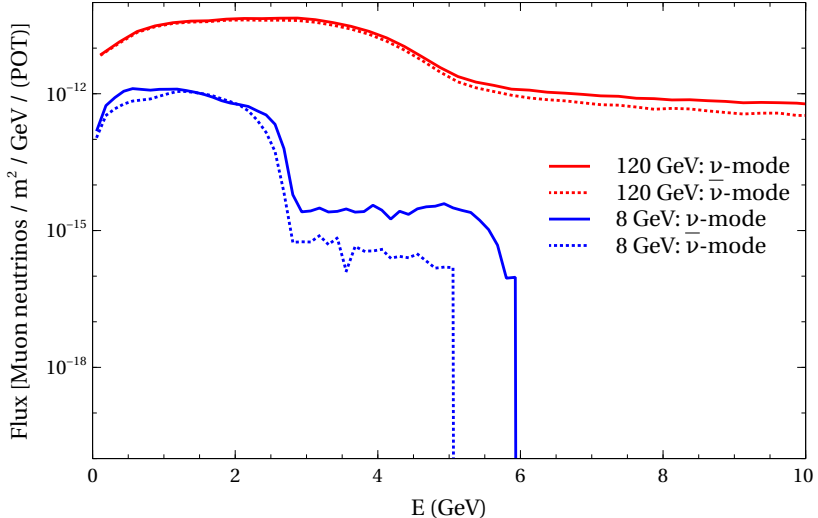


Figure 7: The red and blue curves represent the muon neutrino flux for 120 GeV beam [18, 76] and 8 GeV beam, respectively. The solid and dotted curves indicate flux in neutrino and antineutrino modes, respectively.

2.484 g/cm³, following the PREM profile [78, 79]. Unless otherwise specified, we use the benchmark values for both standard and non-standard neutrino oscillation parameters from Table 1. Throughout this work, we adopt the normal mass ordering (NO) as our default assumption. We marginalize over all standard oscillation parameters (except the Dirac CP violating phase δ and the NSI parameters) to determine the sensitivity. Following experimental specifications, we include a 2% systematic uncertainty on the average matter density, as outlined in the Technical Design Report (TDR).

4 Statistical Analysis

Event Spectrum at DUNE

In this section, we present the expected event spectra at the DUNE far detector for both the SI and NSI scenarios using the GLoBES software. The spectra are shown for a 3.5 year runtime, each for FHC (forward horn current), i.e., neutrino mode, and RHC (reverse horn current), i.e., antineutrino mode, for a total runtime of seven years for both 120 GeV and 8 GeV beams. One of the event spectrum plots is also shown with the optimized runtime combination of both the above mentioned beams, keeping the total runtime fixed, which is discussed in detail in Section 5. Fig. 8 and Fig. 9 show the expected rate of selected events for ν_e (top panel) and $\bar{\nu}_e$ (bottom panel) appearance for of SI (left panel) and NSI (right panel) scenarios, considering expected flux, cross section, and oscillation probabilities as a function of reconstructed neutrino energy at a baseline of 1258 km. In general, one notes that the event spectra are peaked at the value of energy where the flux is optimized. For the 120 GeV beam at the first oscillation maximum, the events peak around 2.6 GeV, while for the 8 GeV beam at the second oscillation maximum, it is around 0.8 – 0.9 GeV.

The signal for ν_e appearance is an excess of charged current (CC) ν_e and $\bar{\nu}_e$ interactions over the expected background in the far detector. The background to the ν_e appearance is composed of

- Beam $(\nu_e + \bar{\nu}_e)$ CC : CC interactions of ν_e and $\bar{\nu}_e$ intrinsic to the beam;
- $(\nu_\tau + \bar{\nu}_\tau)$ CC : ν_τ and $\bar{\nu}_\tau$ CC events in which the τ 's decay leptonically into electrons/positrons.
- $(\nu_\mu + \bar{\nu}_\mu)$ CC : misidentified ν_μ and $\bar{\nu}_\mu$ CC events;
- NC: neutral current backgrounds.

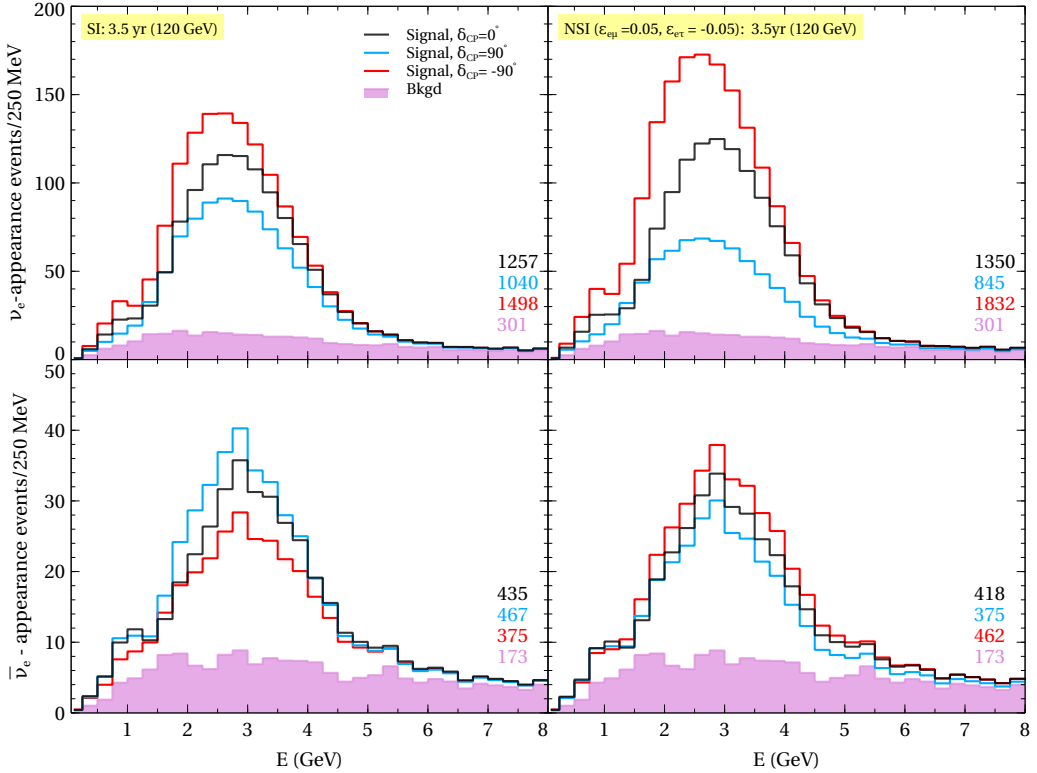


Figure 8: Event spectra of 120 GeV beam for ν_e appearance (top panel) and $\bar{\nu}_e$ appearance (bottom panel) with SI (left panel) and NSI (right panel) with a runtime of 3.5 years in each mode.

In each event spectrum figure, we display the signal for $\delta = 0^\circ$, $\pi/2$, and $-\pi/2$, along with the total backgrounds. We can clearly see that the event rate for $\delta = -\pi/2$ is larger than for $\delta = \pi/2$ in neutrino mode, with the reverse being true for antineutrino mode. Both the signal and the backgrounds are larger in neutrino mode than in antineutrino mode. In the presence of NSI ($\epsilon_{e\mu} = 0.05$ and $\epsilon_{e\tau} = -0.05$), the signal increases for $\delta = -\pi/2$ and decreases for $\delta = \pi/2$, regardless of the beam mode. Statistically, the 8 GeV beam performs worse than the 120 GeV beam. However, due to its importance in determining CP violation sensitivities at the second oscillation maximum, combining the

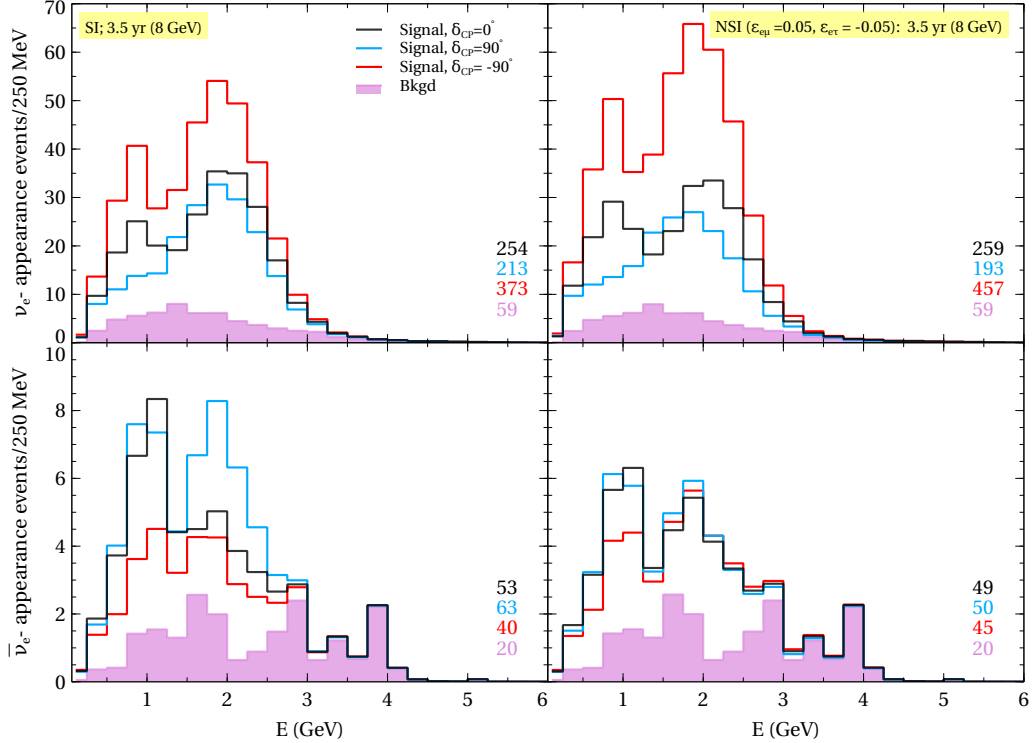


Figure 9: Event spectra of 8 GeV beam for ν_e appearance (top panel) and $\bar{\nu}_e$ appearance (bottom panel) with SI (left panel) and NSI (right panel) with a runtime of 3.5 years in each mode.

Physics Scenarios	120 GeV: ν_e ($\bar{\nu}_e$) app	8 GeV: ν_e ($\bar{\nu}_e$) app	120 GeV + 8 GeV: ν_e ($\bar{\nu}_e$) app
Event rate for SI			
Signal $\delta = 0$	1257 (435)	254 (53)	1865 (123)
Signal $\delta = \pi/2$	1040 (467)	213 (63)	1543 (133)
Signal $\delta = -\pi/2$	1498 (375)	373 (40)	2243 (106)
Total Bkgd	301 (173)	59 (20)	445 (49)
Event rate for NSI			
Signal $\delta = 0$	1350 (418)	259 (49)	1998 (119)
Signal $\delta = \pi/2$	845 (375)	193 (50)	1259 (106)
Signal $\delta = -\pi/2$	1832 (462)	457 (45)	2744 (131)
Total Bkgd	301 (173)	59 (20)	445 (49)

Table 2: Total number of event rates of appearance channel for all three beam options with SI and NSI.

two beams may yield better results than using the standard 120 GeV beam alone. The optimal runtime combination for both beams, determined by optimizing the CP violation sensitivity at DUNE (see Section 5), is found to be 5 years in neutrino mode and 1 year in antineutrino mode for the 120 GeV beam, plus 1 year in neutrino mode only for the 8 GeV beam. This keeps the total runtime fixed at 7 years. The event rate for the combined beams is shown in Fig. 10.

Table 2 shows the integrated event rates for the total signal and background in the ν_e ($\bar{\nu}_e$) appearance channel in neutrino (antineutrino) mode, considering both SI and NSI. The total rates are integrated over the reconstructed neutrino energy range used in this

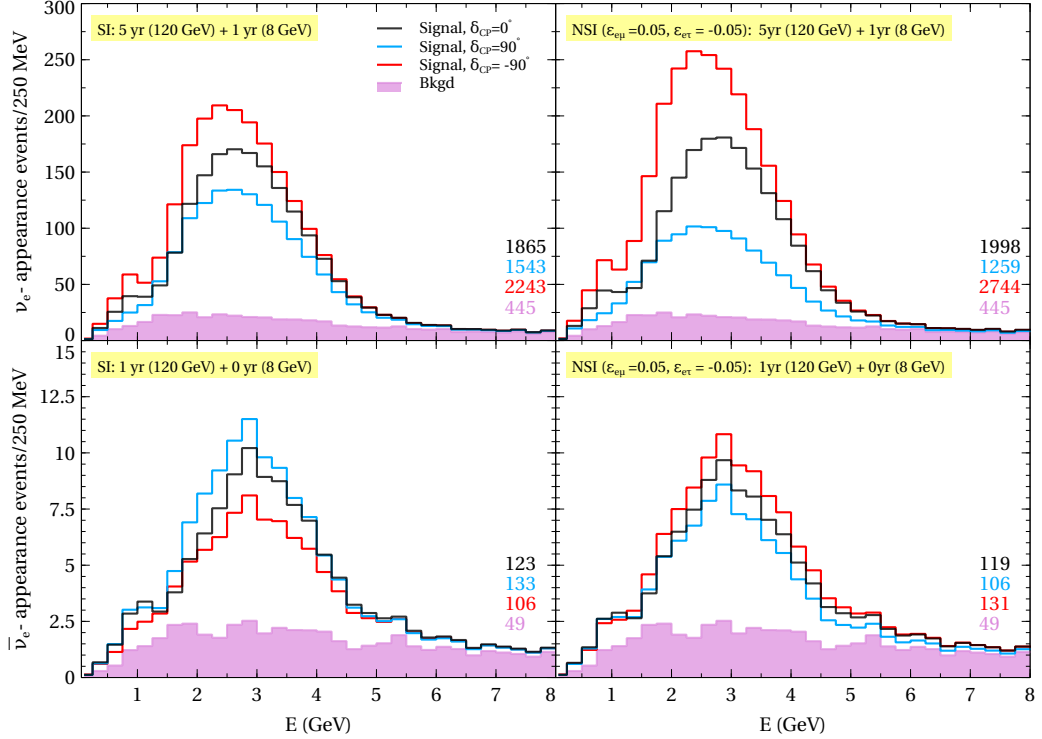


Figure 10: Event spectra of combination of 8 GeV and 120 GeV beams for ν_e appearance (top panel) and $\bar{\nu}_e$ appearance (bottom panel) with SI (left panel) and NSI (right panel) with runtimes as mentioned in the figure.

analysis, 0.5-8 GeV. The event spectra for SI and NSI clearly show that NSI significantly increases the ν_e appearance event rate. However, the rate of increment is smaller in the $\bar{\nu}_e$ appearance channel, implying that NSI has a more pronounced effect on neutrinos than on antineutrinos compared to the SI case. For the NSI case at $\delta = -\pi/2$, the signal improves relative to SI by 334 (87), 84 (5), and 501 (25) events for the 120 GeV, 8 GeV, and combined beams, respectively, in neutrino mode (antineutrino mode). In contrast, a reduction occurs at $\delta_{CP} = \pi/2$, with 195 (92), 20 (13), and 284 (27) fewer events for the same beam configurations.

5 Sensitivity Analysis

DUNE is designed to explore leptonic CP violation within the standard three flavor neutrino oscillation framework. A conclusive signal of CP violation requires the true value of δ to differ significantly from the CP conserving values 0 and π . To quantify the experiment's ability to discriminate between CP violating and CP conserving scenarios, we define the statistical measure χ^2 as

$$\chi^2 \equiv \min_{\delta_{\text{test}}} \sum_{i=1}^x \sum_{j=\nu, \bar{\nu}} \frac{[N_{\text{true}}^{i,j}(\delta_{\text{true}}) - N_{\text{true}}^{i,j}(\delta_{\text{true}} = 0, \pi)]^2}{N_{\text{true}}^{i,j}(\delta_{\text{true}})}. \quad (5.1)$$

In this expression, $N_{\text{true}}^{i,j}$ and $N_{\text{test}}^{i,j}$ represent the predicted event counts for the (i,j) th energy bin and neutrino/antineutrino mode, respectively. The index i runs over the reconstructed energy bins ($i = 1, \dots, N_x$), where the binning scheme is experiment dependent. For DUNE, the binning consists of 64 bins of width 125 MeV in the 0-8 GeV region, along with seven wider bins covering 8-20 GeV. The second index j sums over both neutrino and antineutrino channels [25]. It is important to note that we employ the Pearson definition of the test statistic, for which $\Delta\chi^2 = \chi^2$ and the corresponding significance is given by $N_\sigma = \sqrt{\Delta\chi^2}$. This choice is appropriate since no statistical fluctuations are included in the simulated event samples. For sufficiently large data sets, the alternative definition based on the log-likelihood formalism yields numerically comparable results.

The CP violation discovery potential for a given true value of the phase, δ_{true} , is evaluated through the quantity

$$\Delta\chi^2 = \min[\Delta\chi^2(\delta_{\text{true}} = 0), \Delta\chi^2(\delta_{\text{true}} = \pi)] , \text{ where } \Delta\chi^2 = \chi_{\delta_{\text{test}}}^2 - \chi_{\delta_{\text{true}}}^2.$$

A larger value of $\Delta\chi^2$ indicates a greater ability to reject the CP conserving hypotheses and therefore a stronger sensitivity to leptonic CP violation.

To evaluate the sensitivity to CP violation, we construct the test statistic χ^2 under the assumption of CP conservation. In this framework, the test values of the CP violating phase are fixed to $\delta = 0$ or π , representing the two CP conserving hypotheses. The corresponding χ^2 is then computed for each possible true value of the phase within the full physical interval $\delta \in [-\pi, \pi]$. This approach enables us to quantify how effectively a given experimental setup can distinguish CP violating values of δ from the CP conserving cases.

The characteristic double peak structure visible in Fig. 11 reflects the minimization over the test parameters for a specific set of true oscillation parameters. This procedure is repeated over the entire range of true parameter values. In addition, the total sensitivity is obtained by summing the χ^2 contributions from both the appearance channel ($\nu_\mu \rightarrow \nu_e$) and the disappearance channel ($\nu_\mu \rightarrow \nu_\mu$). Including both channels ensures that the sensitivity estimate fully incorporates the complementary information provided by the two oscillation modes.

5.1 CP violation sensitivity

With the event rates and spectral features characterized, we turn to a key objective of long-baseline experiments: probing CP violation in the neutrino sector. We analyze DUNE's capability to measure the CP violating phase δ and study how the presence of NSI parameters modifies this sensitivity. The left panel of Fig. 11 shows the resulting CP violation sensitivity as a function of the true value of δ for several representative beam configurations. The blue curve corresponds to the 8 GeV beam, while the red and green curves correspond to the 120 GeV and combined (8 + 120) GeV beam options, respectively. Throughout this analysis, we adopt $\varepsilon_{e\mu} = 0.05$ and $\varepsilon_{e\tau} = -0.05$ as benchmark NSI values and marginalize over the standard oscillation parameters when computing the sensitivity. As expected, the sensitivity peaks near $\delta = \pm 90^\circ$, the points of maximal CP violation, for both SI (dashed curves) and NSI (solid curves). This reflects the larger statistical separation between the

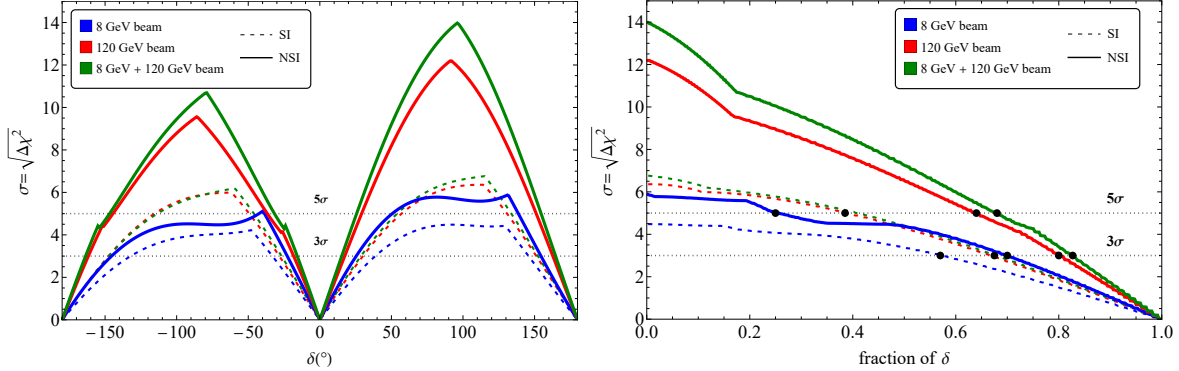


Figure 11: Upper panel shows the significance of the DUNE determination of CP violation as a function of the true value of δ for seven years exposure equally distributed in both neutrino and anti-neutrino mode for SI (right panel) and for NSI (left panel). Sensitivity to CP violation as a function of the fraction of values of δ for NSI (left panel) and for SI (right panel).

event spectra at $\delta = \pm 90^\circ$ and those at the CP conserving values $\delta = 0$ or π . The 8 GeV beam, which mainly probes the second oscillation maximum, does not reach the 5σ level across the full range of δ under SI, even with improved energy resolution. However, in the presence of NSI, the same beam achieves sensitivities slightly above 5σ , underscoring the enhanced CP violating effects induced by NSI at lower energies. The 120 GeV beam, centered near the first oscillation maximum, provides a significantly stronger CP violation reach, exceeding 5σ for SI and surpassing 10σ for the benchmark NSI scenario.

A notable improvement occurs when the 8 GeV and 120 GeV beams are combined (green curve). Using 6 years of exposure for the 120 GeV beam (5 years in ν mode and 1 year in $\bar{\nu}$ mode) together with 1 year of 8 GeV running (1 year in ν mode), the CP violation sensitivity experiences a substantial enhancement in the presence of NSI. While this configuration does not yield a significant improvement beyond the 120 GeV beam alone for the SI case, it becomes essential once NSI effects are included, pushing the sensitivity beyond the 12σ level. This reflects the complementary roles played by the first and second oscillation maxima, demonstrating the advantage of a dual-beam strategy for maximizing CP violation discovery potential in NSI scenarios.

5.2 Fractional CP violation sensitivity

The right panel of Fig. 11 presents the same sensitivity information as the left panel, but expressed in terms of the fraction of CP phase values for which CP violation can be established at a given confidence level. This representation provides a complementary perspective by quantifying how much of the δ parameter space is experimentally accessible.

For the 8 GeV beam (blue curve), the SI scenario (dashed line) allows CP violation to be discovered at the 3σ level for about 56% of all possible δ values, though no region reaches 5σ . In contrast, when NSI are included (solid line), the same beam configuration achieves 5σ discovery for roughly 24% of the δ range, reflecting the enhanced CP violating effects induced by NSI near the second oscillation maximum.

For the SI case, the 120 GeV beam (red curve) and the optimized combined 8 GeV + 120 GeV configuration (green curve) yield similar performance. CP violation can be established at the 3σ (5σ) level for about 67% (40%) of the δ values. However, the impact of NSI is much more pronounced. With NSI, the 120 GeV beam alone provides sensitivity at the 3σ (5σ) level over approximately 80% (64%) of the parameter space, while the combined configuration extends this coverage to nearly 85% (70%).

These results align with the event rate analysis. The presence of NSI enhances the ν_e appearance rate in the neutrino mode by modifying the matter affected oscillation probabilities. This enhancement directly strengthens the CP violation discovery reach, particularly for the combined (8 + 120) GeV beam, where the contributions from the first and second oscillation maxima complement each other most effectively. Overall, the fractional coverage perspective underscores the robustness of DUNE's CP violation sensitivity and highlights the importance of optimized dual beam strategies, especially in scenarios where NSI effects are present.

6 Conclusion

The present study investigates the impact of NSI in the context of DUNE, specifically focusing on the extraction of intrinsic CP violation effects within the three flavor neutrino oscillation framework. A key aspect of this analysis is the significance of the second oscillation maximum in the measurement of the CP violating phase δ in the presence of NSI. Our results demonstrate that, in the presence of NSI, the oscillation probability $P_{\mu e}$ for the channel $\nu_\mu \rightarrow \nu_e$ at the second oscillation maximum exhibits a significant enhancement compared to both the vacuum and standard matter interaction cases. This enhancement directly correlates with an increase in the CP violation term $\Delta P_{\mu e}^{CP}$, as illustrated in Fig. 3. The figure explicitly highlights that the inclusion of NSI amplifies CP violation most prominently in the region of the second oscillation maximum. Consequently, this region emerges as an optimal probe for investigating CP violation in the neutrino sector under NSI effects. However, it is essential to recognize that CP violation in neutrino oscillations is inherently entangled with matter effects. This interplay presents a challenge in isolating the intrinsic CP violation component, particularly in the presence of NSI. Previous studies have explored the extraction of intrinsic CP violation under standard matter interactions, leveraging the parameter, $\delta(\Delta P_{\mu e}) = \Delta P_{\mu e}(\delta = \pi/2) - \Delta P_{\mu e}(\delta = 0)$ to eliminate fake CP effects induced by matter interactions. While this approach enhances the prospects for identifying intrinsic CP violation, the incorporation of NSI complicates the extraction process, as clearly depicted in the oscillogram plots of Fig. 4. Despite the disruption of the symmetric structure of intrinsic CP violation under NSI, our analysis suggests that its extraction remains viable, particularly in the vicinity of CP conserving regions. To facilitate this, we introduce the parameter $\delta(\Delta P^{CP}) = \Delta P^{CP}(\delta) - \Delta P^{CP}(\delta = 0)$, which enhances the feasibility of isolating intrinsic CP violation. Fig. 5 further reinforces the advantage of the second oscillation maximum in minimizing matter effects. Notably, in the neighborhood of the CP conserving region ($\delta = \pm 20^\circ$), our results indicate a promising avenue for extracting intrinsic CP violation even in the presence of NSI.

The probability level analysis reveals that, in the presence of NSI, the appearance probability of electron neutrinos is significantly enhanced at $\delta = -90^\circ$. This enhancement has a pronounced impact on the CP violating term $\Delta P_{\mu e}$, which attains its maximal value at $\delta = -90^\circ$. The effect progressively amplifies from vacuum to standard matter interactions and further in the presence of NSI. However, at $\delta = -90^\circ$, the extraction of intrinsic CP violation becomes increasingly challenging due to the entanglement of matter effects with the CP phase. This complexity arises from the difficulty in isolating the genuine CP violating contribution from the fake CP effects induced by the matter potential. Consequently, while maximal CP violation can be achieved at $\delta = -90^\circ$ in the region of the second oscillation maximum under NSI, precise determination of δ remains nontrivial. Nevertheless, the vicinity of the CP conserving region ($\delta = \pm 20^\circ$) provides a viable avenue for extracting information about the intrinsic CP phase. In this region, the matter effects are relatively minimized, thereby improving the prospects for disentangling the intrinsic CP violation from background contributions.

The statistical analysis corroborates this observation. In the presence of SI, approximately 1478 ν_e events are observed at $\delta = -90^\circ$. This number is effectively reduced to 496 in the ν mode in the presence of NSI, indicating a significant effect. The effective reduction in the event rate strengthens the prospects of probing CP violation under the influence of NSI, offering a more comprehensive understanding of the underlying physics.

We find that DUNE can achieve high significance sensitivity to leptonic CP violation over a wide range of the Dirac phase. In the SI scenario (dashed line), the 120 GeV beam (red line in Fig. 11) alone surpasses 5σ sensitivity near $\delta = \pm\pi/2$, while the 8 GeV beam (blue line in Fig. 11) contributes mainly at the second oscillation maximum without reaching discovery level. In the presence of NSI (solid line), however, the 120 GeV beam yields sensitivity above 10σ , and the optimized (8 + 120) GeV configuration (green line in Fig. 11) further extends the coverage beyond 12σ , enabling CP violation discovery for nearly 70% of the δ parameter space at 5σ . These results establish the complementarity of the first and second oscillation maxima and underscore the importance of optimized combined beam strategies for maximizing DUNE’s discovery potential, especially under nonstandard interaction effects.

The fractional sensitivity study shows that DUNE can establish leptonic CP violation over a substantial portion of the parameter space. In the SI case, the 120 GeV beam alone covers about 40% of δ values at 5σ , while in the presence of NSI, this coverage increases to nearly 64%. The optimized (8 + 120) GeV beam configuration further enhances discovery potential, extending the 5σ reach to about 70% of the δ range. These results demonstrate the robustness of DUNE’s capability to probe CP violation and highlight the essential role of combined beam strategies, particularly when NSI effects are considered.

In summary, our study demonstrates that while NSI substantially modify the extraction of intrinsic CP violation, the second oscillation maximum at DUNE remains a powerful probe to recover sensitivity. These results underscore the necessity of carefully incorporating NSI effects in future precision analyses and highlight the complementary role of multiple oscillation maxima in advancing our understanding of CP violation in the neutrino sector.

ACKNOWLEDGMENTS

RB would like to thank the Ministry of Electronics and IT for the financial support through the Visvesvaraya fellowship scheme for carrying out this research work. The use of HPC cluster at SPS, JNU funded by DST-FIST is acknowledged. JR would like to thank OSHEC (Odisha State Higher Education Council) for the financial support through Mukhyamantri Research Innovation (MRI) for Extramural Research Funding 2023. SP acknowledges the financial support under MTR/2023/000687 funded by SERB, Government of India. The research of PM is supported in part by the Inter-University Centre for Astronomy and Astrophysics (IUCAA), Pune through its Associateship Programme. PM would like to acknowledge IIT Kanpur for kind hospitality during the finishing stages of this work. This work reflects the views of the authors and not those of the DUNE collaboration.

Appendix

A Standard three flavor neutrino oscillation

In the standard three flavor framework, the evolution equation for neutrinos is

$$i \frac{d}{dt} \begin{pmatrix} \nu_e \\ \nu_\mu \\ \nu_\tau \end{pmatrix} = \left[\frac{1}{2E} U \begin{pmatrix} 0 & 0 & 0 \\ 0 & \Delta m_{21}^2 & 0 \\ 0 & 0 & \Delta m_{31}^2 \end{pmatrix} U^\dagger + \begin{pmatrix} V_{CC} & 0 & 0 \\ 0 & 0 & 0 \\ 0 & 0 & 0 \end{pmatrix} \right] \begin{pmatrix} \nu_e \\ \nu_\mu \\ \nu_\tau \end{pmatrix}. \quad (\text{A.1})$$

Here, $\Delta m_{ij}^2 = m_i^2 - m_j^2$ denotes the mass-squared difference with $i, j = 1, 2, 3$ ($i \neq j$), E denotes the neutrino energy, and V_{CC} is the charged current (CC) matter potential defined by

$$V_{CC} = \sqrt{2} G_F N_e \simeq 7.6 \times Y_e \times \frac{\rho}{10^{14} \text{g/cm}^3} \text{ eV}, \quad (\text{A.2})$$

where G_F is the Fermi coupling constant, ρ is the matter density, and $Y_e = N_e/(N_p + N_n)$ is the electron fraction. N_e is the electron number density while N_p and N_n are the proton and neutron number densities respectively. For an electrically neutral and isoscalar medium, $N_e = N_p = N_n$ and then $Y_e \simeq 0.5$ [35]. Earth matter density, which for DUNE we take as $\rho = 2.848 \text{ gm/cm}^3$.

B Brief review of $\Delta P_{\mu e}^{CP}$ in vacuum and matter

$\Delta P_{\mu e}^{CP}$ in vacuum

In absence of the matter potential the factor f takes the form simply $f_v = f \equiv \sin \Delta$ modifying the P_0 term to $P_0^v = 4s_{13}^2 s_{23}^2 f_v^2$. The probability in vacuum can thus be written as

$$P_{\mu e} = 4s_{13}^2 s_{23}^2 \sin^2 \Delta + 8s_{13}s_{12}c_{12}s_{23}c_{23}\alpha \sin \Delta \cos(\Delta + \delta)$$

where the factor $g \rightarrow 1$ in the vacuum limit, and $f = \frac{\sin[(1-v)\Delta]}{1-v} \rightarrow \sin \Delta$. Similarly, the appearance probability for antineutrinos, accounting for δ , flip $\delta \rightarrow -\delta$ is given by

$$\bar{P}_{\mu e} = 4s_{13}^2 s_{23}^2 \sin^2 \Delta + 8s_{13}s_{12}c_{12}s_{23}c_{23}\alpha \sin \Delta \cos(\Delta - \delta)$$

Therefore, the intrinsic CP violation in neutrino oscillation in vacuum is given by

$$\Delta P_{\mu e}^{CP} = 16s_{13}s_{12}c_{12}s_{23}c_{23}\alpha \sin^2 \Delta \sin \delta \quad (B.1)$$

It is evident that the expression for CP violation in vacuum, representing the intrinsic CP violation in the neutrino sector, exhibits a sinusoidal dependence on the CP phase δ [25, 32].

$\Delta P_{\mu e}^{CP}$ in matter

With the inclusion of matter effects, the factor f in the transition probability expression for neutrinos modifies as $f = \sin[(1-v)\Delta]/(1-v)$ and for the antineutrino $f' = \sin[(1+v)\Delta]/(1+v)$. Meanwhile, the factor $g = \sin v\Delta/v$ remains unchanged for both neutrinos and anti-neutrinos. Therefore, in the presence of matter potential, the neutrino appearance probability takes the form

$$P_{\mu e} = P_0 + P_1 = 4s_{13}^2s_{23}^2f^2 + 8s_{13}s_{12}c_{12}s_{23}c_{23}\alpha fg \cos(\Delta + \delta)$$

while the anti-neutrino probability is given by

$$\bar{P}_{\mu e} = 4s_{13}^2s_{23}^2(f')^2 + 8s_{13}s_{12}c_{12}s_{23}c_{23}\alpha f'g \cos(\Delta - \delta).$$

The CP asymmetry in the presence of matter effects is thus expressed as

$$\Delta P_{\mu e}^{CP} = 4s_{13}^2s_{23}^2(f^2 - f'^2) + 8s_{13}s_{12}c_{12}s_{23}c_{23}g \left[\cos \Delta(f - f') \cos \delta - (f + f') \sin \Delta \sin \delta \right] \quad (B.2)$$

In the presence of SI with the matter potential, the CP violation term exhibits both *sine* and *cosine* dependencies on the CP phase δ . However, at the oscillation maxima, the *cosine* contribution vanishes, resulting in $\Delta P_{\mu e}^{CP}$ showing a pure dependence *sinusoidal* on the intrinsic CP phase δ .

References

- [1] B. Pontecorvo, *Inverse Beta Processes and Nonconservation of Lepton Charge*, Sov. Phys. JETP **7** (1958) 172–173.
- [2] B. Pontecorvo, *Mesonium and Antimesonium*, Sov. Phys. JETP **6** (1958) 429–431.
- [3] B. Pontecorvo, *Neutrino Experiments and the Problem of Conservation of Leptonic Charge*, Zh. Eksp. Teor. Fiz. **53** (1967) 1717–1725.
- [4] V. Gribov and B. Pontecorvo, *Neutrino astronomy and lepton charge*, Phys. Lett. B **28** (1969) 493.
- [5] Z. Maki, M. Nakagawa, and S. Sakata, *Remarks on the unified model of elementary particles*, Prog. Theor. Phys. **28** (1962) 870–880.
- [6] T. Kajita and A. B. McDonald, “For the discovery of neutrino oscillations, which shows that neutrinos have mass.” The Nobel Prize in Physics 2015. <https://www.nobelprize.org/prizes/physics/2015/summary/>.

[7] P. F. de Salas, D. V. Forero, S. Gariazzo, P. Martínez-Miravé, O. Mena, C. A. Ternes, M. Tórtola, and J. W. F. Valle, *2020 global reassessment of the neutrino oscillation picture*, *JHEP* **02** (2021) 071, [[arXiv:2006.11237](https://arxiv.org/abs/2006.11237)].

[8] F. Capozzi, W. Giarè, E. Lisi, A. Marrone, A. Melchiorri, and A. Palazzo, *Neutrino masses and mixing: Entering the era of subpercent precision*, *Phys. Rev. D* **111** (2025), no. 9 093006, [[arXiv:2503.07752](https://arxiv.org/abs/2503.07752)].

[9] I. Esteban, M. C. Gonzalez-Garcia, M. Maltoni, I. Martinez-Soler, J. P. Pinheiro, and T. Schwetz, *NuFit-6.0: updated global analysis of three-flavor neutrino oscillations*, *JHEP* **12** (2024) 216, [[arXiv:2410.05380](https://arxiv.org/abs/2410.05380)].

[10] Y. Farzan and M. Tortola, *Neutrino oscillations and Non-Standard Interactions*, *Front. in Phys.* **6** (2018) 10, [[arXiv:1710.09360](https://arxiv.org/abs/1710.09360)].

[11] B. Dasgupta and J. Kopp, *Sterile Neutrinos*, *Phys. Rept.* **928** (2021) 1–63, [[arXiv:2106.05913](https://arxiv.org/abs/2106.05913)].

[12] **DUNE** Collaboration, B. Abi et al., *Prospects for beyond the Standard Model physics searches at the Deep Underground Neutrino Experiment*, *Eur. Phys. J. C* **81** (2021), no. 4 322, [[arXiv:2008.12769](https://arxiv.org/abs/2008.12769)].

[13] **Particle Data Group** Collaboration, S. Navas et al., *Review of particle physics*, *Phys. Rev. D* **110** (2024), no. 3 030001.

[14] M. Fukugita and T. Yanagida, *Baryogenesis Without Grand Unification*, *Phys. Lett. B* **174** (1986) 45–47.

[15] S. Davidson, E. Nardi, and Y. Nir, *Leptogenesis*, *Phys. Rept.* **466** (2008) 105–177, [[arXiv:0802.2962](https://arxiv.org/abs/0802.2962)].

[16] **DUNE** Collaboration, R. Acciari et al., *Long-Baseline Neutrino Facility (LBNF) and Deep Underground Neutrino Experiment (DUNE): Conceptual Design Report, Volume 2: The Physics Program for DUNE at LBNF*, [arXiv:1512.06148](https://arxiv.org/abs/1512.06148).

[17] **DUNE** Collaboration, B. Abi et al., *Long-baseline neutrino oscillation physics potential of the DUNE experiment*, *Eur. Phys. J. C* **80** (2020), no. 10 978, [[arXiv:2006.16043](https://arxiv.org/abs/2006.16043)].

[18] **DUNE** Collaboration, B. Abi et al., *Deep Underground Neutrino Experiment (DUNE), Far Detector Technical Design Report, Volume II: DUNE Physics*, [arXiv:2002.03005](https://arxiv.org/abs/2002.03005).

[19] **Hyper-Kamiokande** Collaboration, K. Abe et al., *Hyper-Kamiokande Design Report*, [arXiv:1805.04163](https://arxiv.org/abs/1805.04163).

[20] **Hyper-Kamiokande** Collaboration, K. Abe et al., *Physics potentials with the second Hyper-Kamiokande detector in Korea*, *PTEP* **2018** (2018), no. 6 063C01, [[arXiv:1611.06118](https://arxiv.org/abs/1611.06118)].

[21] **KM3Net** Collaboration, S. Adrian-Martinez et al., *Letter of intent for KM3NeT 2.0*, *J. Phys. G* **43** (2016), no. 8 084001, [[arXiv:1601.07459](https://arxiv.org/abs/1601.07459)].

[22] A. V. Akindinov et al., *Letter of Interest for a Neutrino Beam from Protvino to KM3NeT/ORCA*, *Eur. Phys. J. C* **79** (2019), no. 9 758, [[arXiv:1902.06083](https://arxiv.org/abs/1902.06083)].

[23] M. Bishai, M. Diwan, S. Kettell, J. Stewart, B. Viren, E. Worcester, R. Tschirhart, and L. Whitehead, *Precision Neutrino Oscillation Measurements using Simultaneous High-Power, Low-Energy Project-X Beams*, in *Snowmass 2013: Snowmass on the Mississippi*, 7, 2013. [arXiv:1307.0807](https://arxiv.org/abs/1307.0807).

[24] M. Bass et al., *Baseline Optimization for the Measurement of CP Violation, Mass Hierarchy, and θ_{23} Octant in a Long-Baseline Neutrino Oscillation Experiment*, *Phys. Rev. D* **91** (2015), no. 5 052015, [[arXiv:1311.0212](https://arxiv.org/abs/1311.0212)].

[25] J. Rout, S. Shafaq, M. Bishai, and P. Mehta, *Physics prospects with the second oscillation maximum at the Deep Underground Neutrino Experiment*, *Phys. Rev. D* **103** (2021), no. 11 116003, [[arXiv:2012.08269](https://arxiv.org/abs/2012.08269)].

[26] L. Wolfenstein, *Neutrino Oscillations in Matter*, *Phys. Rev. D* **17** (1978) 2369–2374.

[27] Y. Grossman, *Nonstandard neutrino interactions and neutrino oscillation experiments*, *Phys. Lett. B* **359** (1995) 141–147, [[hep-ph/9507344](https://arxiv.org/abs/hep-ph/9507344)].

[28] N. Fornengo, M. Maltoni, R. Tomas, and J. W. F. Valle, *Probing neutrino nonstandard interactions with atmospheric neutrino data*, *Phys. Rev. D* **65** (2002) 013010, [[hep-ph/0108043](https://arxiv.org/abs/hep-ph/0108043)].

[29] M. Blennow, T. Ohlsson, and W. Winter, *Non-standard Hamiltonian effects on neutrino oscillations*, *Eur. Phys. J. C* **49** (2007) 1023–1039, [[hep-ph/0508175](https://arxiv.org/abs/hep-ph/0508175)].

[30] S. Antusch, J. P. Baumann, and E. Fernandez-Martinez, *Non-Standard Neutrino Interactions with Matter from Physics Beyond the Standard Model*, *Nucl. Phys. B* **810** (2009) 369–388, [[arXiv:0807.1003](https://arxiv.org/abs/0807.1003)].

[31] D. Meloni, T. Ohlsson, and H. Zhang, *Exact and Approximate Formulas for Neutrino Mixing and Oscillations with Non-Standard Interactions*, *JHEP* **04** (2009) 033, [[arXiv:0901.1784](https://arxiv.org/abs/0901.1784)].

[32] A. M. Gago, H. Minakata, H. Nunokawa, S. Uchinami, and R. Zukanovich Funchal, *Resolving CP Violation by Standard and Nonstandard Interactions and Parameter Degeneracy in Neutrino Oscillations*, *JHEP* **01** (2010) 049, [[arXiv:0904.3360](https://arxiv.org/abs/0904.3360)].

[33] R. Adhikari, S. Chakraborty, A. Dasgupta, and S. Roy, *Non-standard interaction in neutrino oscillations and recent Daya Bay, T2K experiments*, *Phys. Rev. D* **86** (2012) 073010, [[arXiv:1201.3047](https://arxiv.org/abs/1201.3047)].

[34] S. K. Agarwalla, F. Lombardi, and T. Takeuchi, *Constraining Non-Standard Interactions of the Neutrino with Borexino*, *JHEP* **12** (2012) 079, [[arXiv:1207.3492](https://arxiv.org/abs/1207.3492)].

[35] A. Chatterjee, P. Mehta, D. Choudhury, and R. Gandhi, *Testing nonstandard neutrino matter interactions in atmospheric neutrino propagation*, *Phys. Rev. D* **93** (2016), no. 9 093017, [[arXiv:1409.8472](https://arxiv.org/abs/1409.8472)].

[36] S. Choubey and T. Ohlsson, *Bounds on Non-Standard Neutrino Interactions Using PINGU*, *Phys. Lett. B* **739** (2014) 357–364, [[arXiv:1410.0410](https://arxiv.org/abs/1410.0410)].

[37] S. K. Agarwalla, P. Bagchi, D. V. Forero, and M. Tórtola, *Probing Non-Standard Interactions at Daya Bay*, *JHEP* **07** (2015) 060, [[arXiv:1412.1064](https://arxiv.org/abs/1412.1064)].

[38] T. Ohlsson, H. Zhang, and S. Zhou, *Nonstandard interaction effects on neutrino parameters at medium-baseline reactor antineutrino experiments*, *Phys. Lett. B* **728** (2014) 148–155, [[arXiv:1310.5917](https://arxiv.org/abs/1310.5917)].

[39] S. Choubey, A. Ghosh, T. Ohlsson, and D. Tiwari, *Neutrino Physics with Non-Standard Interactions at INO*, *JHEP* **12** (2015) 126, [[arXiv:1507.02211](https://arxiv.org/abs/1507.02211)].

[40] M. Masud, A. Chatterjee, and P. Mehta, *Probing CP violation signal at DUNE in presence of non-standard neutrino interactions*, *J. Phys. G* **43** (2016), no. 9 095005, [[arXiv:1510.08261](https://arxiv.org/abs/1510.08261)].

- [41] A. de Gouv  a and K. J. Kelly, *Non-standard neutrino interactions at DUNE*, *Nucl. Phys. B* **908** (2016) 318–335, [[arXiv:1511.05562](https://arxiv.org/abs/1511.05562)].
- [42] P. Coloma, *Non-Standard Interactions in propagation at the Deep Underground Neutrino Experiment*, *JHEP* **03** (2016) 016, [[arXiv:1511.06357](https://arxiv.org/abs/1511.06357)].
- [43] M. Masud and P. Mehta, *Nonstandard interactions spoiling the CP violation sensitivity at DUNE and other long baseline experiments*, *Phys. Rev. D* **94** (2016) 013014, [[arXiv:1603.01380](https://arxiv.org/abs/1603.01380)].
- [44] M. Masud and P. Mehta, *Nonstandard interactions and resolving the ordering of neutrino masses at DUNE and other long baseline experiments*, *Phys. Rev. D* **94** (2016), no. 5 053007, [[arXiv:1606.05662](https://arxiv.org/abs/1606.05662)].
- [45] S.-F. Ge and A. Y. Smirnov, *Non-standard interactions and the CP phase measurements in neutrino oscillations at low energies*, *JHEP* **10** (2016) 138, [[arXiv:1607.08513](https://arxiv.org/abs/1607.08513)].
- [46] M. Blennow, S. Choubey, T. Ohlsson, D. Pramanik, and S. K. Raut, *A combined study of source, detector and matter non-standard neutrino interactions at DUNE*, *JHEP* **08** (2016) 090, [[arXiv:1606.08851](https://arxiv.org/abs/1606.08851)].
- [47] K. N. Deepthi, S. Goswami, and N. Nath, *Can nonstandard interactions jeopardize the hierarchy sensitivity of DUNE?*, *Phys. Rev. D* **96** (2017), no. 7 075023, [[arXiv:1612.00784](https://arxiv.org/abs/1612.00784)].
- [48] S. Fukasawa, M. Ghosh, and O. Yasuda, *Sensitivity of the T2HKK experiment to nonstandard interactions*, *Phys. Rev. D* **95** (2017), no. 5 055005, [[arXiv:1611.06141](https://arxiv.org/abs/1611.06141)].
- [49] J. Liao, D. Marfatia, and K. Whisnant, *Nonstandard neutrino interactions at DUNE, T2HK and T2HKK*, *JHEP* **01** (2017) 071, [[arXiv:1612.01443](https://arxiv.org/abs/1612.01443)].
- [50] S. K. Agarwalla, S. S. Chatterjee, and A. Palazzo, *Degeneracy between θ_{23} octant and neutrino non-standard interactions at DUNE*, *Phys. Lett. B* **762** (2016) 64–71, [[arXiv:1607.01745](https://arxiv.org/abs/1607.01745)].
- [51] S. K. Agarwalla, S. S. Chatterjee, A. Dasgupta, and A. Palazzo, *Discovery Potential of T2K and NOvA in the Presence of a Light Sterile Neutrino*, *JHEP* **02** (2016) 111, [[arXiv:1601.05995](https://arxiv.org/abs/1601.05995)].
- [52] J. Rout, M. Masud, and P. Mehta, *Can we probe intrinsic CP and T violations and nonunitarity at long baseline accelerator experiments?*, *Phys. Rev. D* **95** (2017), no. 7 075035, [[arXiv:1702.02163](https://arxiv.org/abs/1702.02163)].
- [53] M. Masud, M. Bishai, and P. Mehta, *Extricating New Physics Scenarios at DUNE with Higher Energy Beams*, *Sci. Rep.* **9** (2019), no. 1 352, [[arXiv:1704.08650](https://arxiv.org/abs/1704.08650)].
- [54] A. Medhi, D. Dutta, and M. M. Devi, *Exploring the effects of scalar non standard interactions on the CP violation sensitivity at DUNE*, *JHEP* **06** (2022) 129, [[arXiv:2111.12943](https://arxiv.org/abs/2111.12943)].
- [55] S. S. Chatterjee, P. S. B. Dev, and P. A. N. Machado, *Impact of improved energy resolution on DUNE sensitivity to neutrino non-standard interactions*, *JHEP* **08** (2021) 163, [[arXiv:2106.04597](https://arxiv.org/abs/2106.04597)].
- [56] B. Brahma and A. Giri, *Exploring non standard interactions effects in T2HK and DUNE*, *Eur. Phys. J. C* **82** (2022), no. 12 1145.
- [57] R. Majhi, D. K. Singha, M. Ghosh, and R. Mohanta, *Distinguishing nonstandard interaction*

and Lorentz invariance violation at the Protvino to super-ORCA experiment, *Phys. Rev. D* **107** (2023), no. 7 075036, [[arXiv:2212.07244](https://arxiv.org/abs/2212.07244)].

[58] A. Sarker, A. Medhi, D. Bezboruah, M. M. Devi, and D. Dutta, *Impact of scalar NSI on the neutrino mass ordering sensitivity at DUNE, HK and KNO*, *JHEP* **06** (2024) 128, [[arXiv:2309.12249](https://arxiv.org/abs/2309.12249)].

[59] A. Sarker, D. Bezboruah, A. Medhi, and M. M. Devi, *Sensitivity of DUNE in the presence of off-diagonal scalar NSI parameters*, *Phys. Rev. D* **112** (2025), no. 3 035042, [[arXiv:2406.15307](https://arxiv.org/abs/2406.15307)].

[60] D. Bezboruah, D. S. Chattopadhyay, A. Medhi, A. Sarker, and M. M. Devi, *Neutrino oscillations in presence of diagonal elements of scalar NSI: an analytic approach*, *JHEP* **12** (2025) 222, [[arXiv:2410.05250](https://arxiv.org/abs/2410.05250)].

[61] A. Medhi, A. Sarker, and M. M. Devi, *Scalar NSI: a unique tool for constraining absolute neutrino masses via neutrino oscillations*, *Eur. Phys. J. C* **85** (2025), no. 4 380, [[arXiv:2307.05348](https://arxiv.org/abs/2307.05348)].

[62] **Super-Kamiokande** Collaboration, G. Mitsuka et al., *Study of Non-Standard Neutrino Interactions with Atmospheric Neutrino Data in Super-Kamiokande I and II*, *Phys. Rev. D* **84** (2011) 113008, [[arXiv:1109.1889](https://arxiv.org/abs/1109.1889)].

[63] **MINOS** Collaboration, P. Adamson et al., *Search for Flavor-Changing Non-Standard Neutrino Interactions by MINOS*, *Phys. Rev. D* **88** (2013), no. 7 072011, [[arXiv:1303.5314](https://arxiv.org/abs/1303.5314)].

[64] C. Biggio, M. Blennow, and E. Fernandez-Martinez, *General bounds on non-standard neutrino interactions*, *JHEP* **08** (2009) 090, [[arXiv:0907.0097](https://arxiv.org/abs/0907.0097)].

[65] C. Biggio, M. Blennow, and E. Fernandez-Martinez, *Loop bounds on non-standard neutrino interactions*, *JHEP* **03** (2009) 139, [[arXiv:0902.0607](https://arxiv.org/abs/0902.0607)].

[66] F. J. Escrivuela, M. Tortola, J. W. F. Valle, and O. G. Miranda, *Global constraints on muon-neutrino non-standard interactions*, *Phys. Rev. D* **83** (2011) 093002, [[arXiv:1103.1366](https://arxiv.org/abs/1103.1366)].

[67] P. Coloma, M. C. Gonzalez-Garcia, M. Maltoni, J. P. Pinheiro, and S. Urrea, *Global constraints on non-standard neutrino interactions with quarks and electrons*, *JHEP* **08** (2023) 032, [[arXiv:2305.07698](https://arxiv.org/abs/2305.07698)].

[68] S. Parveen, K. Sharma, S. Patra, and P. Mehta, *Signals of eV-scale sterile neutrino at long baseline neutrino experiments*, *Eur. Phys. J. C* **85** (2025), no. 2 181, [[arXiv:2305.16824](https://arxiv.org/abs/2305.16824)].

[69] S. Parveen, M. Masud, M. Bishai, and P. Mehta, *Sterile sector impacting the correlations and degeneracies among mixing parameters at the Deep Underground Neutrino Experiment*, *JHEP* **01** (2025) 139, [[arXiv:2409.17878](https://arxiv.org/abs/2409.17878)].

[70] J. Rout, M. Masud, and P. Mehta, *Impact of New Physics on CP-Asymmetries at Long Baselines*, *Springer Proc. Phys.* **203** (2018) 795–797.

[71] P. Coloma, I. Esteban, M. C. Gonzalez-Garcia, and M. Maltoni, *Improved global fit to Non-Standard neutrino Interactions using COHERENT energy and timing data*, *JHEP* **02** (2020) 023, [[arXiv:1911.09109](https://arxiv.org/abs/1911.09109)]. [Addendum: *JHEP* 12, 071 (2020)].

[72] T. Kikuchi, H. Minakata, and S. Uchinami, *Perturbation Theory of Neutrino Oscillation with Nonstandard Neutrino Interactions*, *JHEP* **03** (2009) 114, [[arXiv:0809.3312](https://arxiv.org/abs/0809.3312)].

- [73] P. Huber, M. Lindner, and W. Winter, *Simulation of long-baseline neutrino oscillation experiments with GLoBES (General Long Baseline Experiment Simulator)*, *Comput. Phys. Commun.* **167** (2005) 195, [[hep-ph/0407333](#)].
- [74] P. Huber, J. Kopp, M. Lindner, M. Rolinec, and W. Winter, *New features in the simulation of neutrino oscillation experiments with GLoBES 3.0: General Long Baseline Experiment Simulator*, *Comput. Phys. Commun.* **177** (2007) 432–438, [[hep-ph/0701187](#)].
- [75] A. M. Dziewonski and D. L. Anderson, *Preliminary reference earth model*, *Phys. Earth Planet. Interiors* **25** (1981) 297–356.
- [76] **DUNE** Collaboration, B. Abi et al., *Experiment Simulation Configurations Approximating DUNE TDR*, [arXiv:2103.04797](#).
- [77] J. Kopp, *Sterile neutrinos and non-standard neutrino interactions in globes*, *MPI-HD Technical Report* (2019).
- [78] F. D. Stacey, *Physics of the Earth*. Wiley, 2nd ed., 1977.
- [79] A. M. Dziewonski and D. L. Anderson, *Preliminary reference earth model*, *Physics of the Earth and Planetary Interiors* **25** (June, 1981) 297–356.